

Investigation of NO_x emissions and NO_x-related chemistry in East Asia using CMAQ-predicted and GOME-derived NO₂ columns

K. M. Han¹, C. H. Song¹, H. J. Ahn¹, R. S. Park¹, J. H. Woo², C. K. Lee^{1,3}, A. Richter⁴, J. P. Burrows⁴, J. Y. Kim⁵, and J. H. Hong⁶

¹Dept. of Environmental Science and Engineering, Gwangju Institute of Science and Technology (GIST), Gwangju, Korea

²Department of Advanced Technology Fusion, Konkuk University, Seoul, Korea

³Department of Physics and Atmospheric Science, Dalhousie University, Halifax, Nova Scotia, Canada

⁴Institute of Environmental Physics, University of Bremen, Otto-Hahn-Allee 1, 28359, Bremen, Germany

⁵Hazardous Substance Research Center, Korea Institute of Science and Technology (KIST), Seoul, Korea

⁶Air Pollution Cap System Division, National Institute of Environmental Research (NIER), Incheon, Korea

Received: 21 July 2008 – Published in Atmos. Chem. Phys. Discuss.: 17 September 2008

Revised: 17 December 2008 – Accepted: 7 January 2009 – Published: 11 February 2009

Abstract. In this study, NO₂ columns from the US EPA Models-3/CMAQ model simulations carried out using the 2001 ACE-ASIA (Asia Pacific Regional Aerosol Characterization Experiment) emission inventory over East Asia were compared with the GOME-derived NO₂ columns. There were large discrepancies between the CMAQ-predicted and GOME-derived NO₂ columns in the fall and winter seasons. In particular, while the CMAQ-predicted NO₂ columns produced larger values than the GOME-derived NO₂ columns over South Korea for all four seasons, the CMAQ-predicted NO₂ columns produced smaller values than the GOME-derived NO₂ columns over North China for all seasons with the exception of summer (summer anomaly). It is believed that there might be some error in the NO_x emission estimates as well as uncertainty in the NO_x chemical loss rates over North China and South Korea. Regarding the latter, this study further focused on the biogenic VOC (BVOC) emissions that were strongly coupled with NO_x chemistry during summer in East Asia. This study also investigated whether the CMAQ-modeled NO₂/NO_x ratios with the possibly overestimated isoprene emissions were higher than those with reduced isoprene emissions. Although changes in both the NO_x chemical loss rates and NO₂/NO_x ratios from CMAQ-modeling with the different isoprene emissions affected the CMAQ-modeled NO₂ levels, the effects were found to be limited, mainly due to the low absolute levels of NO₂ in

summer. Seasonal variations of the NO_x emission fluxes over East Asia were further investigated by a set of sensitivity runs of the CMAQ model. Although the results still exhibited the summer anomaly possibly due to the uncertainties in both NO_x-related chemistry in the CMAQ model and the GOME measurements, it is believed that consideration of both the seasonal variations in NO_x emissions and the correct BVOC emissions in East Asia are critical. Overall, it is estimated that the NO_x emissions are underestimated by ~57.3% in North China and overestimated by ~46.1% in South Korea over an entire year. In order to confirm the uncertainty in NO_x emissions, the NO_x emissions over South Korea and China were further investigated using the ACE-ASIA, REAS (Regional Emission inventory in ASia), and CAPSS (Clean Air Policy Support System) emission inventories. The comparison between the CMAQ-calculated and GOME-derived NO₂ columns indicated that both the ACE-ASIA and REAS inventories have some uncertainty in NO_x emissions over North China and South Korea, which can also lead to some errors in modeling the formation of ozone and secondary aerosols in South Korea and North China.

1 Introduction

Nitrogen oxides (NO_x≡NO+NO₂) emitted from anthropogenic sources, such as fossil fuel combustion and biomass burning, as well as natural sources, such as lightning and microbiological processes in soil, play important roles in



Correspondence to: C. H. Song
(chsong@gist.ac.kr)

tropospheric ozone chemistry and secondary aerosol formation. Several studies have focused on NO_x emissions from China to determine their influence on air quality and aerosol radiative forcing in East Asia (e.g., Uno et al., 2007; Wang et al., 2007; Zhang et al., 2007). Recent studies using satellite measurements reported that NO₂ columns (or NO₂ vertical column density, VCD) have increased significantly in East Asia since 2001 (Richter et al., 2005; van der A et al., 2006; He et al., 2007). Such increases in NO_x emissions over China were confirmed partly by a bottom-up emission inventory study (Zhang et al., 2007). In order to test the accuracy of NO_x emissions, several studies were carried out over East Asia comparing the 3-D model-predicted NO₂ columns with satellite-derived NO₂ columns (Kunhikrishnan et al., 2004; Ma et al., 2006; van Noije et al., 2006; Uno et al., 2007). The comparisons revealed large inconsistencies between the NO₂ columns from the 3-D CTM (Chemistry-Transport Model) simulations and the satellite-derived NO₂ columns. For example, Uno et al. (2007) reported that the 3-D CTM-derived NO₂ columns with the REAS (Regional Emission inventory in ASia) emission inventory were lower by a factor of 2–4 over polluted Central East China, compared with the GOME (Global Ozone Monitoring Experiment)-retrieved NO₂ columns. In addition, Ma et al. (2006) also reported that the 3-D CTM-derived NO₂ columns with the ACE-ASIA (Asia Pacific Regional Aerosol Characterization Experiment) emission inventory underestimated the NO_x emissions over China during the summer for the year 2000 by more than 50% compared with the GOME-derived NO₂ columns. However, there has been no detailed investigation carried out as to how and why the NO₂ columns over China were under-predicted by 3-D CTM simulation using the ACE-ASIA or REAS inventory. In addition, there are no reports on the possibly important seasonal (or monthly) variations in NO_x emissions in East Asia and the relationship between the rates of NO_x chemical loss and the fluxes of biogenic isoprene emissions in East Asia, even though they could be important factors for evaluating NO_x emissions. The latter (biogenic emissions) could be important because they can control the levels of OH radicals, which can affect the NO_x chemical loss rates.

On the other hand, an accurate estimation of NO_x emissions in China is important because NO_x emissions from North China tend to persistently affect the air quality of South Korea (e.g., Arndt et al., 1998). From 2003, the Korean government began to implement an ambitious pollution abatement policy that aimed at improving the air quality of Seoul Metropolitan area, called the “Total Air Pollution Load Management System”, by reducing the levels of secondary pollutants, such as O₃, PANs (Peroxy Acetyl Nitrates), and nitrate (Korean Ministry of Environment, 2006). This policy included a specific plan to reduce the total anthropogenic NO_x emissions from the Seoul Metropolitan area by 53%, from 309 387 Ton yr⁻¹ to 145 412 Ton yr⁻¹. The reference and target years for the Total Air Pollution Load Manage-

ment System are 2001 and 2014, respectively. However, the critical and largest uncertainty in implementing this policy is to evaluate and quantify accurately the influences of the emissions outside the policy domain on the air quality of the Seoul Metropolitan area. Due to the strong and persistent source-receptor relationship between North China and South Korea, it is important to use accurate emission inventories for both the source (“North China”) and the receptor regions (“Seoul Metropolitan area” or “South Korea”) for the reference and target years, 2001 and 2014.

This study examined the accuracy of NO_x emissions from North China and South Korea using the CMAQ-simulated and GOME-derived NO₂ columns. In addition to the uncertainty in NO_x emission itself, this paper also discussed the possibly important uncertainty factors that could cause inconsistencies between the CMAQ-derived and GOME-derived NO₂ columns. In particular, both seasonal variations in the NO_x emissions and the HO_x-NO_x-isoprene photochemistry in East Asia were examined in detail on account of its possibly strong relationship with the inconsistency between the CMAQ-simulated and GOME-derived NO₂ columns in East Asia.

2 Experimental methods

In this study, three dimensional Eulerian CTM simulations over East Asia were carried out in conjunction with the Meteorological fields generated from the PSU/NCAR MM5 (Pennsylvania state University/National Center for Atmospheric Research Meso-scale Model 5) model in order to compare the CTM-predicted NO₂ columns with the satellite (GOME)-derived NO₂ columns.

2.1 US EPA Models-3/CMAQ modeling

In this study, a 3-D Eulerian CTM, US EPA Models-3/CMAQ (Community Multi-scale Air Quality) model was used in conjunction with the MET fields generated from PSU/NCAR MM5 modeling over an approximately 3 week period for four seasons: Late Fall (9–27 November 2001), Spring (25 March 2002–13 April 2002), Late Summer (24 August 2002–13 September 2002), and Winter (11–28 February 2003) (Byun and Ching, 1999; Byun and Schere, 2006). The details of the modeling conditions were reported by Song et al. (2008). For the MET fields, the 2.5° × 2.5° resolved re-analyzed National Centers for Environmental Prediction (NCEP) data with automated data processing (ADP) of the global surface and upper air observations were employed using four-dimensional data assimilation (FDDA) techniques (Stauffer and Seaman, 1990, 1994). The MET fields were generated at “1-h intervals” during the four episode periods. The CMAQ modeling system then used the meteorological fields generated from the PSU/NCAR MM5 and emission fields. The schemes selected

in CMAQ modeling are as follows: the piece-wise parabolic method (PPM) for advection (Collela and Woodward, 1984); 4th generation carbon bond mechanism (CBM 4) for gas phase chemistry (Gery et al., 1989); the Carnegie-Mellon University (CMU) aqueous chemistry mechanism for cloud chemistry (Pandis and Seinfeld, 1989; Fahey and Pandis, 2003); the AERO3 module for particulate dynamics and aerosol thermodynamics (Binkowski and Roselle, 2003); and the Wesley scheme for the dry deposition of both gaseous and particulate species (Wesley, 1989). The 4th generation carbon bond mechanism for gas-phase chemistry included explicit VOC species, such as ALD2 (higher aldehyde, C>2), ETH (ethane), FORM (formaldehyde), ISOP (isoprene), OLE (olefin), PAR (paraffin), TOL (toluene), and XYL (xylene). As indicated above, far more detailed atmospheric chemistry and physical processes, aerosol dynamics, and thermodynamic gas-aerosol processes were considered in these calculations than in other global and regional chemistry-transport modeling studies in order to better consider the atmospheric fate of NO_x. For example, in this study the analysis was not restricted to “clear sky conditions”. In other words, it fully considered cloud chemistry, wet scavenging, and the effects of clouds on the photolysis reaction rates.

The horizontal domain of the CMAQ modeling shown in Fig. 1 covered the region from approximately 100° E to 150° E and 20° N to 50° N, which included Korea, Japan, China, and parts of Mongolia and Russia with a 108 km×108 km grid resolution. For vertical resolution, 24 layers were used with σ -coordinates using the model-top at 180 hPa. For comparison, NO₂ vertical column loading was integrated from the surface to 250 hPa (approximately corresponding to ~10 km a.s.l. in these calculations). The CMAQ-modeled NO₂ columns were averaged between 10:00 LST and 12:00 LST because the GOME measurements were taken approximately at 10:30 LST over East Asia. The total number of the grid points in the CMAQ model calculations was 36 432. Figure 1 also shows the four main study regions used for the comparison studies: i) North China (Region A, 30° N–42° N; 110° E–125° E); ii) South China (Region B, 22° N–30° N; 108° E–122° E); iii) South Korea (Region C, 33.5° N–40° N; 125° E to 130° E); and iv) Japan (Region D, 31° N–40° N; 130° E–142° E). Here, the remote continental areas in China were excluded from our analysis, partly because they are remote areas, and the NO₂ columns showed a similar order of magnitude of the absolute errors to the GOME measurements (~10¹⁵ molecules cm⁻²).

2.2 Emissions

Emission is an important input parameter in a modeling study. Poor agreement between 3-D modeling studies and satellite measurements is expected if the emission inventories incorrectly reflect the seasonal and spatial emission fluxes from the various sources. In order to consider anthro-

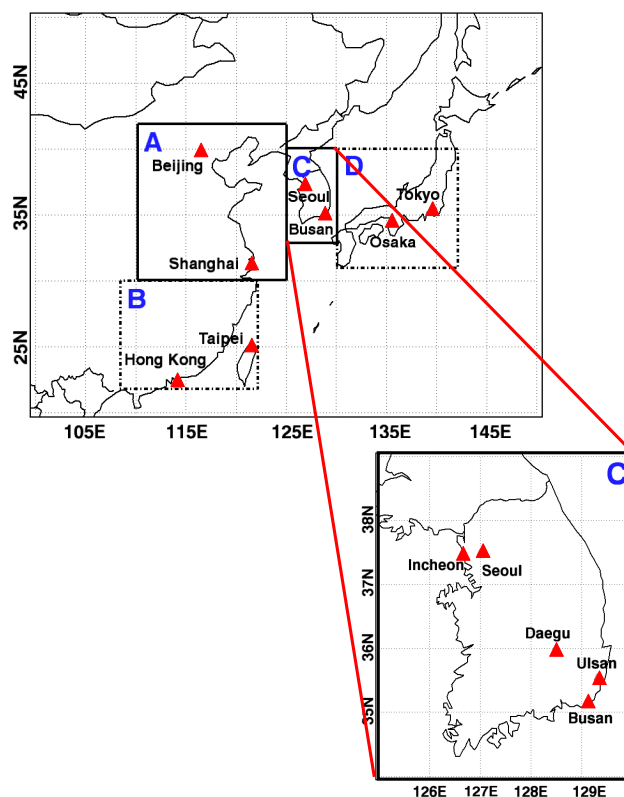


Fig. 1. Modeling domain of the study. Four regions were defined: i) A: North China, ii) B: South China, iii) C: South Korea, and iv) D: Japan.

pogenic emissions, 1°×1° resolved emission data for 9 major species, including SO₂, NO_x, CO, NMVOCs (Non-Methane Volatile Organic Compounds), CH₄, NH₃, CO₂, BC, and OC, were obtained from the official ACE-ASIA and TRACE-P (Transport and Chemical Evaluation over Pacific) emission web site at the University of Iowa (http://www.cgrer.uiowa.edu/EMISSION_DATA/index.htm). Streets et al. (2003) provided detailed information on the emission inventory (hereafter, labeled the ACE-ASIA inventory) used in this study. The ACE-ASIA emission inventory included NO_x emissions from fossil fuels and bio-fuel combustion as well as biomass (vegetation) burning in East Asia. However, the inventory did not consider the NO_x emissions from lightning and microbial activity in soil. In general, emission from lightning is believed to make a small contribution to the total NO_x budget (Martin et al., 2003). On the other hand, Wang et al. (2007) reported that soil NO_x emissions might be important, accounting for up to ~43% of the combustion source during summer in East Asia. In addition, the original ACE-ASIA emission inventory was built up for the year 2000. Therefore, the NO_x emissions for East Asia were modified slightly by multiplying a factor of 1.05 in order to account for an annual increase in NO_x emissions from China for the year 2001 (Zhang et al., 2007).

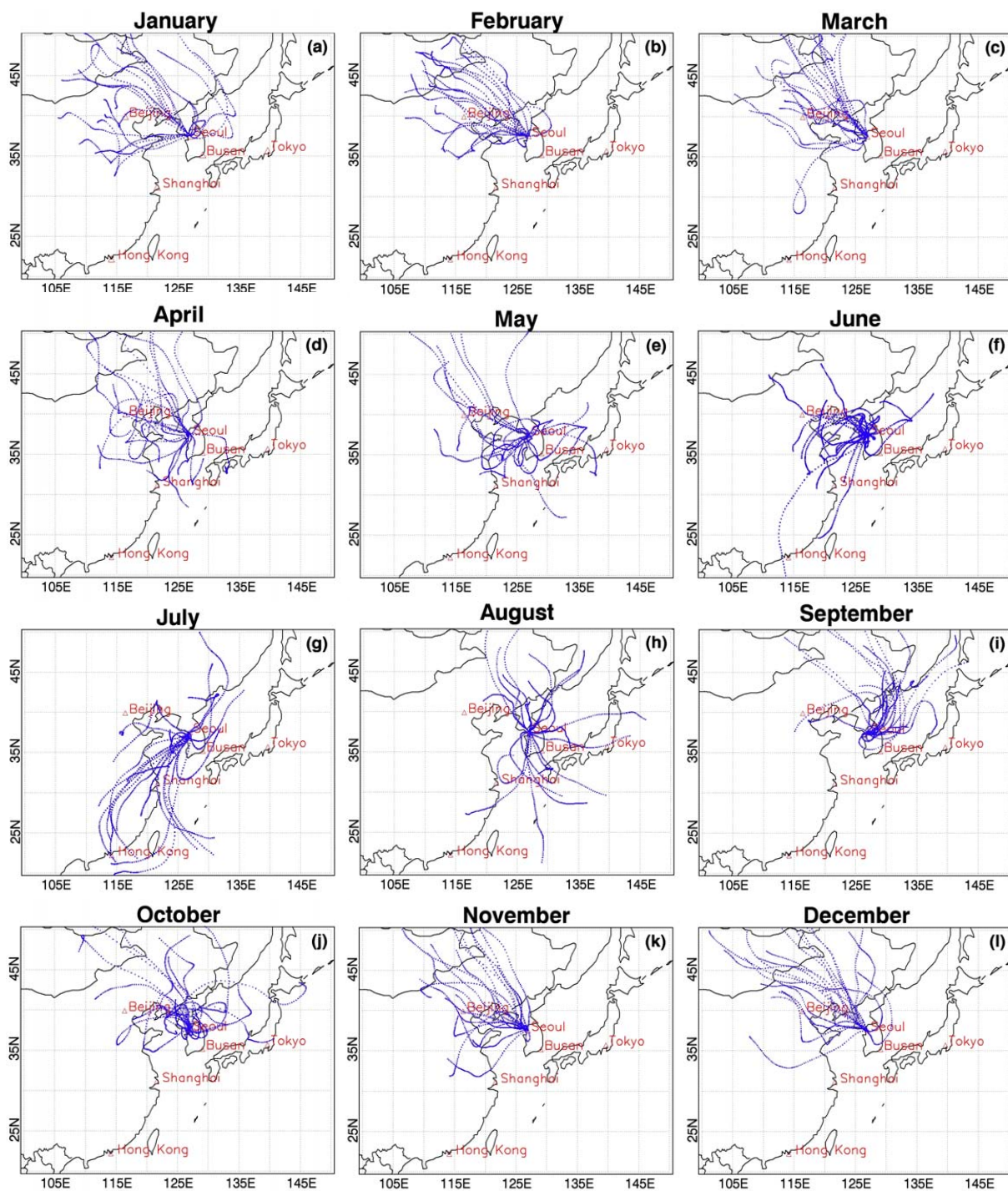


Fig. 2. Three-day backward trajectory analysis for air masses arriving in Seoul, Korea in 2001. The trajectories are obtained at 1 km a.s.l., and are shown at 1 h intervals: (a) January, (b) February, (c) March, (d) April, (e) May, (f) June, (g) July, (h) August, (i) September, (j) October, (k) November, and (l) December.

Anthropogenic NMVOC emissions were assumed to be constant without any seasonal variation. In this study, chemical speciation (chemical species splitting) of the total NMVOC emissions in East Asia was performed using

the SPECIATE database built up by the US EPA. The major biogenic $1^\circ \times 1^\circ$ resolved emissions data of isoprene and monoterpene were obtained from the Global Emissions Inventory Activity (GEIA, <http://geiacenter.org/presentData/>

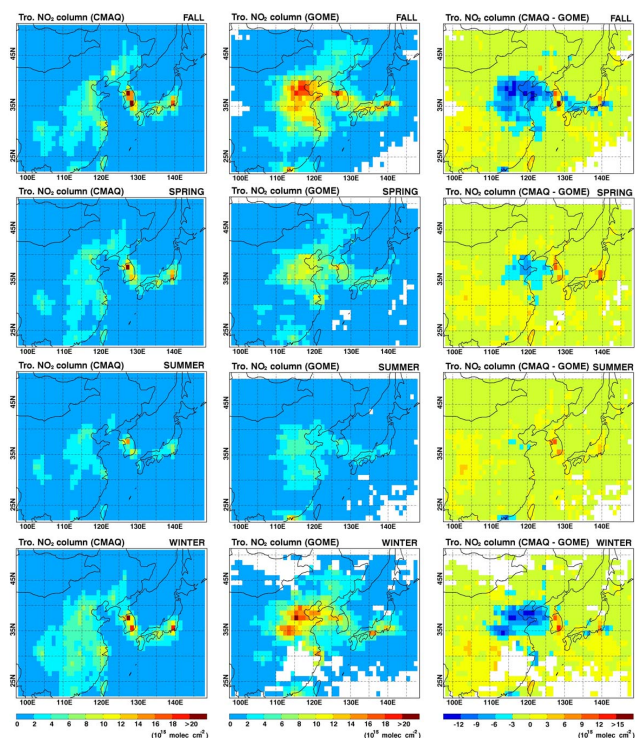


Fig. 3. Seasonal variations in the CMAQ-derived NO₂ columns (unit: $\times 10^{15}$ molecules cm^{-2}) in the first column and GOME-derived NO₂ columns in the second column (unit: $\times 10^{15}$ molecules cm^{-2}). The differences between the CMAQ-derived and GOME-derived NO₂ columns are shown in the third column.

nvoc.html), which was created as an activity of the International Geosphere-Biosphere Program (IGBP).

2.3 NO₂ retrieval algorithm from ESA/ERS-2 GOME platform

GOME was launched on the ERS-2 satellite by European Space Agency (ESA) in April 1995. It is a nadir-scanning double-monochromator, and obtains approximately 30 000 radiance spectra each day covering the ultraviolet and visible wavelengths from 240 to 790 nm at a moderate spectral resolution of 0.17 to 0.33 nm. Because GOME is a nadir viewing instrument, both tropospheric and stratospheric absorptions contribute to the measured signals. The ground scene of GOME typically has a footprint of $320 \times 40 \text{ km}^2$. Total ground coverage is obtained within 3 days at the equator with a 960 km wide track swath (4.5 s forward scan and 1.5 s backward scan).

The NO₂ analysis for GOME is based on a Differential Optical Absorption Spectroscopy (DOAS) retrieval method (Richter and Burrows, 2002; Richter et al., 2005). The wavelength range of 425–450 nm was used for the NO₂ DOAS fit because the differential absorption is large and interference by other species is small. In addition to the NO₂ cross-

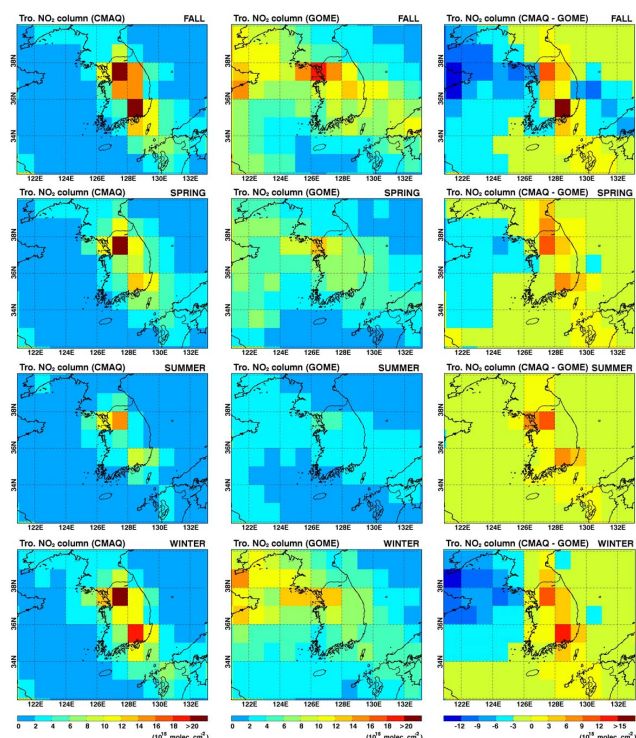


Fig. 4. As Fig. 3, except for closing in South Korea.

section (Burrows et al., 1998), the cross-sections of O₃ (Burrows et al., 1999), O₄ (Greenblatt et al., 1990), H₂O (Rothman et al., 1992), a synthetic Ring spectrum (Vountas et al., 1998), and an undersampling correction (Chance, 1998) were included in the fit. In order to calculate the tropospheric NO₂ slant column, the stratospheric contribution of NO₂ to the measured slant column was removed by subtracting the slant column taken on the same day at the same latitude in the 180°–230° longitude region from the total slant column using the reference sector method (Richter and Burrows, 2002). Cloud screening was applied to remove measurements with a cloud fraction >0.3 , as determined from the GOME measurements using the FRESCO (Fast Retrieval Scheme for Clouds from the Oxygen A-band) algorithm (Koелеmeijer et al., 2001). The tropospheric slant column was then converted to a vertical tropospheric column using the appropriate air mass factor (AMF). The AMF is defined as the ratio of the observed slant column to the vertical column and was calculated with using the radiative transfer model (SCIATRAN) (Rozanov et al., 1997). The monthly averaged AMF on a $2.5^\circ \times 2.5^\circ$ grid was determined using the NO₂ vertical profiles (shape factor) from a global chemical transport model, MOZART-2 (Model for Ozone and Related Tracers).

The error budget of satellite measurements of tropospheric NO₂ columns from GOME has been discussed in detail (e.g. Richter and Burrows, 2002; Martin et al., 2003; Boersma et al., 2004; Richter et al., 2005; van Noije et al., 2006). The main contributions to the error

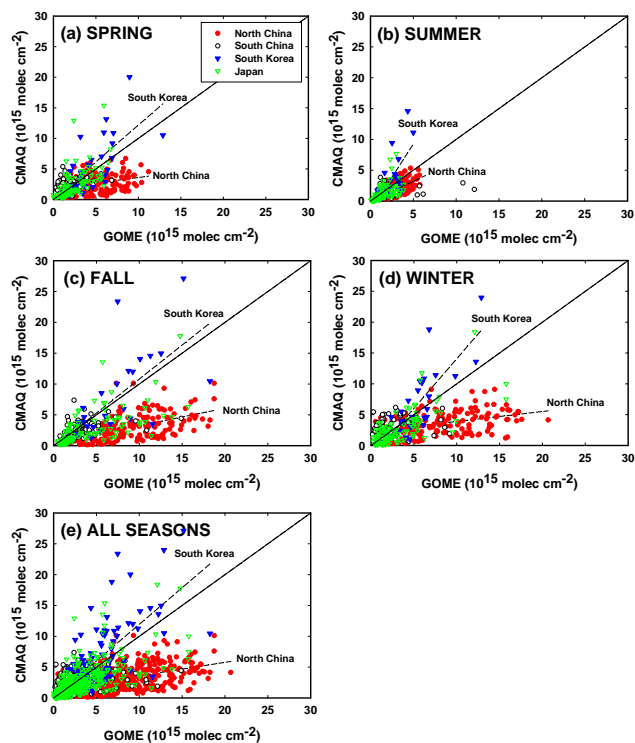


Fig. 5. Scatter plots between the CMAQ-derived and GOME-derived NO_2 columns for (a) spring, (b) summer, (c) fall, (d) winter, and (e) all seasons. North China (red circles), South China (open circles), South Korea (blue triangles), and Japan (green triangles).

are slant column fitting uncertainties, uncertainties related to the subtraction of the stratospheric contributions, uncertainties from residual clouds, and AMF. For an individual GOME pixel, the slant column fitting uncertainties were 2×10^{14} – 4×10^{14} molecules cm^{-2} and the uncertainties in the subtraction of the stratospheric contribution were $< 1 \times 10^{15}$ molecules cm^{-2} (Richter and Burrows, 2002). These values can be reduced further by averaging the space or time. In remote regions, the retrieval errors were dominated by uncertainties in the slant column fitting and the subtraction of the stratospheric contributions. However, these uncertainties are relatively small in polluted regions. The total uncertainties in the retrieval of tropospheric NO_2 columns over continental polluted regions is largely determined by the AMF calculation due to surface reflectivity, clouds, aerosols, and the trace gas profile (Richter et al., 2005; van Noije et al., 2006). An overall assessment of errors leads to 5×10^{14} – 1×10^{15} molecules cm^{-2} for additive error and 40–60% for relative error for the monthly averages over polluted areas (Richter and Burrows, 2002; Richter et al., 2005). More detailed error and uncertainty analysis of the GOME NO_2 columns can be found in the previous publications (Richter and Burrows, 2002; Martin et al., 2003; Boersma et al., 2004; Richter et al., 2005; van Noije et al., 2006).

3 Results and discussions

In order to properly determine the contributions from North China emissions to air quality of South Korea, it is important to evaluate the accuracy of the NO_x emission inventories over both regions and understand NO_x -related gas-phase chemistry. Initially, 3-day backward trajectory analysis was conducted (Sect. 3.1) to confirm the strong source-receptor relationship between North China (A) and South Korea (C). Subsequently, the CMAQ-predicted NO_2 columns are then spatially and seasonally compared with the GOME-derived NO_2 columns (Sect. 3.2). The ACE-ASIA NO_x emissions in North China (A, source region) and South Korea (C, receptor region) are then compared with other recently-released inventories such as, REAS, “date-back” ANL (Argonne National Laboratory) inventory, and CAPSS (Sect. 3.3).

3.1 Backward trajectory analysis

In this study, a 3-day backward trajectory analysis for each month of 2001 was carried out using the NOAA HYSPLIT model (Draxler, 1998) to confirm the persistent source (North China, A)-receptor (South Korea, C) relationship, as well as to determine how frequently the air masses travel from North China (A) to South Korea (C). Approximately 20 days per month were selected. The trajectory ends at a point (37.5°N , 127.0°E) at an altitude of 1 km under which Seoul is located. As shown in Fig. 2, the air masses traveled from North China (A) to South Korea (C) during almost the entire year. However, in July, the air masses appear to be affected by the emissions from South China (B). In August and September, the air masses arrive in Seoul from the North, East, South (August) and the Northeast (September). Although air masses do not always travel from North China (A) to Seoul during July, August, and September, it is clear that the South Korean air quality is most strongly and persistently affected by the emissions from North China (A) throughout almost the entire year. Therefore, in the framework of the source-receptor relationship, this study focused particularly on the emissions from two regions, North China (A) and South Korea (C).

3.2 CMAQ-predicted and GOME-derived NO_2 columns, NO_x emissions, and NO_x -related chemistry in East Asia

3.2.1 CMAQ-predicted vs. GOME-derived NO_2 columns

Figure 3 shows the spatial distributions of the CMAQ-predicted NO_2 columns and the GOME-derived NO_2 columns for four episodes over East Asia. Figure 4 shows a close-up of the area of South Korea for better visualization. There were large discrepancies between the two quantities in the late fall and winter seasons (i.e. cold seasons), as well as strong seasonal variations, particularly in the GOME-derived NO_2 columns. Interestingly, the CMAQ-predicted NO_2 columns were larger than the GOME-derived

NO₂ columns for all seasons over South Korea (C) (Fig. 4). On the other hand, the CMAQ-calculated NO₂ columns over North China (A) were smaller than the GOME-derived NO₂ columns for all seasons except for summer (Fig. 3). Note that the differences between the CMAQ-calculated and the GOME-derived NO₂ columns in the third column in Figs. 3 and 4 have negative values (“blue colors”) over North China (A) and positive values (“red-orange colors”) over South Korea (C). Scatter plots between the CMAQ-predicted and GOME-derived NO₂ columns were also made for North China (A), South China (B), South Korea (C), and Japan (D) for further confirmation. Figure 5 shows that there are no clear seasonal trends in South China (B) and Japan (D), whereas the CMAQ-predicted NO₂ columns over South Korea (C) are obviously larger than the GOME-derived NO₂ columns for all seasons. In addition, the CMAQ-predicted NO₂ columns over North China (A) were clearly smaller than the GOME-derived NO₂ columns for all seasons except for summer. These results are further confirmed through statistical analyses (see Sect. 3.2.2). These results suggest that there are some errors in the estimations of NO_x emissions over North China (A) and South Korea (C) in the ACE-ASIA NO_x emission inventory. Of course, this inference should be valid only when the following assumption is held: In CMAQ modeling, emission is the largest uncertainty, and the other atmospheric chemical and physical processes are reasonably accurate. In this study, we chose the GOME-derived NO₂ columns as reference values, although the GOME measurements also have uncertainties, as discussed in Sect. 2.3, mainly from the assumptions made in the radiative transfer calculations (Richter et al., 2005). In this study, we focused on the highly polluted East Asian regions where the monthly averages of NO₂ columns reach $\sim 2 \times 10^{16}$ molecules cm⁻² (see Figs. 3, 4, and 5; also refer to van Noije et al., 2006 and Uno et al., 2007). The NO₂ columns are larger than the magnitudes of overall errors of the GOME NO₂ column measurements, $0.5 \times 10^{15} - 1 \times 10^{15}$ molecules cm⁻². An attempt was also made to determine why the difference between the CMAQ-predicted and GOME-derived NO₂ columns became minimal only during summer in Fig. 3. This issue is discussed in detail in Sect. 3.2.3.

3.2.2 Statistical analysis

Table 1 shows the seasonal and regional statistical analyses between the CMAQ-predicted and GOME-derived NO₂ columns. The following four statistical parameters were introduced for statistical analyses: i) Root Mean Square Error (RMSE, absolute error); ii) Mean Normalized Gross Error (MNGE, relative error); iii) Mean Bias (MB, absolute bias); and iv) Mean Normalized Bias (MNB, relative bias). The four statistical parameters are defined in Eqs. (1) to (4):

$$\text{RMSE} = \sqrt{\frac{1}{N} \sum_1^N (\text{NO}_{2,\text{CMAQ}} - \text{NO}_{2,\text{GOME}})^2} \quad (1)$$

Table 1. Statistical analysis for the comparisons between the CMAQ-predicted and GOME-derived NO₂ columns over East Asia.

			RMSE ¹	MNGE ²	MB ¹	MNB ²
CMAQ vs. GOME	A	SPRING	3.14	50.94	-1.99	-26.99
		SUMMER	1.39	39.54	-1.00	-32.82
		FALL	6.67	66.42	-5.73	-65.61
		WINTER	6.05	63.34	-4.43	-36.28
B	SPRING	1.21	71.90	0.28	50.95	
	SUMMER	1.65	41.65	-0.72	-24.05	
	FALL	1.82	34.24	-0.53	-6.26	
	WINTER ³	-	-	-	-	
C	SPRING	3.08	44.34	0.86	17.30	
	SUMMER	2.54	48.59	0.81	24.70	
	FALL	4.35	38.44	0.38	0.98	
	WINTER	3.47	37.85	1.06	13.9	
D	SPRING	1.81	88.67	-0.00037	41.64	
	SUMMER	1.04	51.88	-0.23	20.85	
	FALL	3.04	50.88	-1.44	-29.47	
	WINTER	2.23	63.76	-0.61	-1.67	

A: North China; B: South China; C: South Korea; D: Japan

¹ Unit, $\times 10^{15}$ molecules cm⁻²

² Unit, %

³ Due to missing values

$$\text{MNGE} = \frac{1}{N} \sum_1^N \left(\frac{|\text{NO}_{2,\text{CMAQ}} - \text{NO}_{2,\text{GOME}}|}{\text{NO}_{2,\text{GOME}}} \right) \times 100 \quad (2)$$

$$\text{MB} = \frac{1}{N} \sum_1^N (\text{NO}_{2,\text{CMAQ}} - \text{NO}_{2,\text{GOME}}) \quad (3)$$

$$\text{MNB} = \frac{1}{N} \sum_1^N \left(\frac{\text{NO}_{2,\text{CMAQ}} - \text{NO}_{2,\text{GOME}}}{\text{NO}_{2,\text{GOME}}} \right) \times 100 \quad (4)$$

In Table 1, RMSE analysis showed that the magnitudes of the “absolute” differences were much larger over North China (A) and South Korea (C) than over South China (B) and Japan (D) (These are denoted as “bold fonts” in Table 1). Large uncertainties are expected over North China (A) and South Korea (C). The MNGEs range from 39.6% to 66.4% over North China (A) and from 37.9% to 48.6% over South Korea (C). Bias analysis (MB and MNB) showed that the CMAQ-predicted NO₂ columns tend to have positive biases, compared with the GOME-derived NO₂ columns over South Korea (C). In contrast, over North China (A), the CMAQ-predicted NO₂ columns tend to have negative biases. These statistical analyses are also in line with the results reported in Sect. 3.2.1.

3.2.3 Summer anomaly in NO₂ columns over East Asia

The first and second columns in Fig. 3 show seasonal variations of the NO₂ columns over East Asia. The CMAQ-derived NO₂ columns show relatively weak seasonal variations in North China (Region A), whereas the

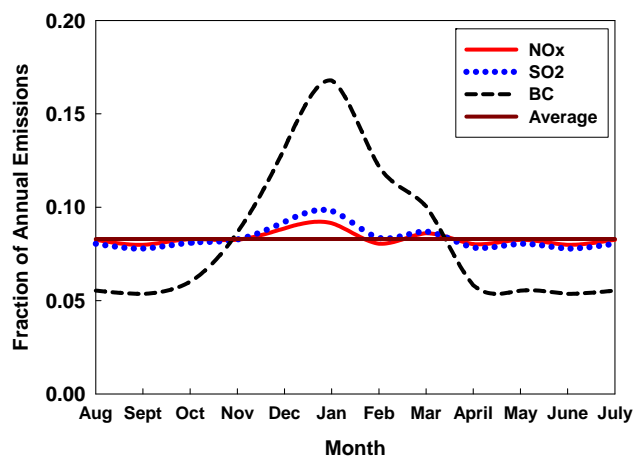


Fig. 6. Seasonal variations in the anthropogenic NO_x (red thick line), SO₂ (blue dot line), and BC (black dash line) emissions in China (Streets et al., 2003).

GOME-derived NO₂ columns show strong seasonal variations. The differences between the two NO₂ columns reduce to almost zero during summer, and are also small over North China (A) during spring (Fig. 3). There are two main factors that may be involved in these phenomena: i) seasonal variations in NO_x emissions; and ii) seasonal variations in the NO_x chemical loss rates. First, the distribution of NO₂ columns can be influenced by the seasonal variations in NO_x emissions. Streets et al. (2003) reported almost no seasonal variations in anthropogenic NO_x and SO₂ emissions, which is in contrast to black carbon (BC) emissions. The monthly fraction of the NO_x emissions is almost constant, as shown in Fig. 6, even though the fractions of NO_x emissions increase slightly in December and January. If this is true, then the seasonal changes in NO_x emissions are not a likely cause of the seasonal variations in the NO₂ columns (Note that uniform NO_x emission fluxes were also assumed in the CMAQ model runs based on the almost constant NO_x emissions shown in Fig. 6). However, the issue of seasonal variations in NO_x emissions in East Asia will be revisited, and explored further in Sect. 3.2.4). Secondly, in order to explain this anomalous (or unexpected) phenomenon in NO₂ columns, this study examined the seasonal variations in NO_x chemical loss rates in East Asia. The chemical mechanisms for NO_x loss are HNO₃, nitrate, and organic nitrate formation (i.e. N(V) formation) in the atmosphere. The N(V) forms from NO_x by reactions (R1) through (R9):

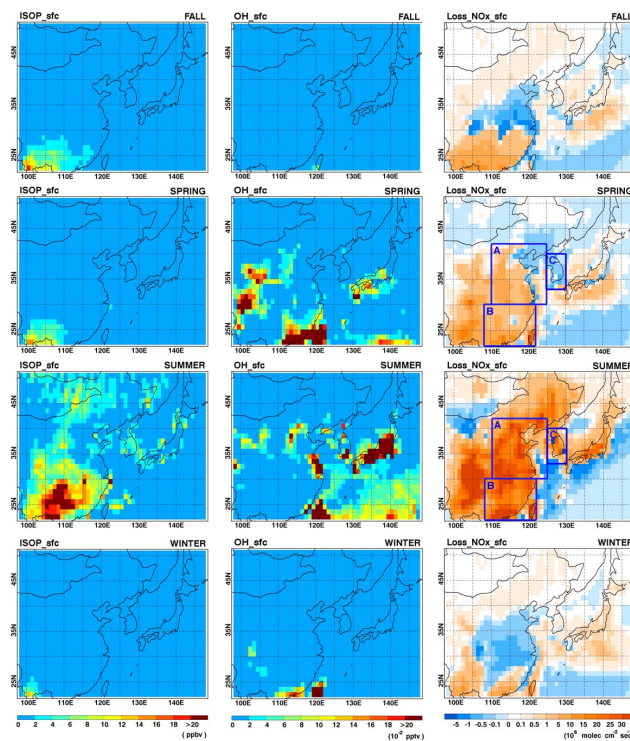
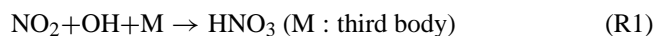
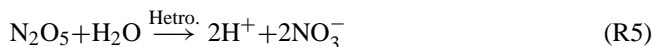


Fig. 7. Seasonal variations in the CMAQ-derived isoprene concentration (unit: \times ppb) at the surface level (the first column), CMAQ-derived hydroxyl radical (OH) concentration (unit: $\times 10^{-2}$ ppt) at the surface level (the second column), and NO_x chemical loss rates (unit: $\times 10^6$ molecules $\text{cm}^{-3} \text{s}^{-1}$) at the surface level (the third column).



Therefore, the NO_x chemical loss rate (L_{NO_x}) can be constructed by Eq. (5) (Song et al., 2003):

$$L_{\text{NO}_x} \equiv k_1 [\text{NO}_2] [\text{OH}] + k_2 [\text{NO}_3] [\text{HCHO}] + k_3 [\text{NO}_3] [\text{ALD2}] + k_{4,h} [\text{NO}_3] + 2k_{5,h} [\text{N}_2\text{O}_5] + k_6 [\text{NO}_2] [\text{CH}_3\text{C}(\text{O})\text{O}_2] + k_8 [\text{NO}_2] [\text{RO}] + k_9 [\text{NO}] [\text{RO}_2] - k_7 [\text{PAN}] \quad (5)$$

where, the first, second and third terms in the right hand side of Eq. (5) represent the NO_x chemical loss rate due to HNO₃ formation via reactions (R1), (R2), and (R3), respectively. The fourth and fifth terms represent heterogeneous nitrate formation by reactions (R4) and (R5), respectively. In Eq. (5), the heterogeneous mass transfer coefficients (s^{-1}) of $k_{4,h}$ and $k_{5,h}$ for NO₃ and N₂O₅ radicals were calculated using the Schwartz formula ($k_i = \gamma_i S_i v_i / 4$) (Schwartz, 1986).

In the Schwartz formula, γ_i , S_i , and v_i represent the reaction probability, aerosol surface density ($\mu\text{m}^2 \text{cm}^{-3}$), and molecular mean velocity (cm s^{-1}) for species i , respectively. Since PAN is a temporary reservoir of NO_x, both the production and decomposition terms of PAN (i.e., R6 and R7) were considered in Eq. (5). In addition, in summer organic nitrate (denoted as RONO₂ in the text and NTR in the CBM4 mechanism of the CMAQ model) formation is important (R8 and R9). Therefore, both reactions were taken into account. Here, R represents the organic functional group.

Among the eight pathways for removing NO_x, L_{NO_x} is influenced mainly by (R1), (R5), and (R9) in Eq. (5) (particularly, (R1) and (R5) during winter and (R1) and (R9) during summer). The third column in Fig. 7 shows the model-predicted, spatial distributions of the NO_x chemical loss rates at the surface. As expected, the rates of NO_x loss are much faster during summer than during the other seasons. However, Fig. 7 shows an unexpected phenomenon. The OH levels in spring are, on average, higher than those in summer over China. It is believed that this may be caused by active biogenic VOC (BVOC) emissions in summer (the anthropogenic NMVOC emissions were kept constant in the CMAQ model runs for the four episodes without seasonal variations). The first column in Fig. 7 shows the biogenic isoprene concentrations at the surface for the four episodes. The isoprene concentrations were highest during summer. The biogenic isoprene emissions influence the formation of ozone, and affect rates of NO_x removal by controlling the levels of hydroxyl radicals.

Hydroxyl radicals (OH) are produced by O^{1D}+H₂O reaction and HONO photo-dissociation. Hydroxyl radicals (OH) are converted to perhydroxyl radicals (HO₂) or organic peroxy radicals (RO₂) through reactions with CO, CH₄, and VOCs. Formaldehydes (HCHO) are also an important source of hydroxyl radicals in that perhydroxyl radicals (HO₂) are produced by HCHO photo-dissociation and HCHO+OH reaction. Perhydroxyl radicals (HO₂) or organic peroxy radicals (RO₂) convert NO to NO₂, and are converted back to hydroxyl radicals (OH). Figure 8 gives an illustration of these relationships. Most importantly, the isoprene emissions can create a shift in the HO_x cycle. Excessive amounts of isoprene (C₅H₈) can deplete OH radicals, producing HO₂ or RO₂ through reaction with excessive isoprene. Subsequently, under the isoprene-abundant environment, HO₂ and RO₂ radicals are removed from the atmosphere producing two products, hydrogen peroxides (H₂O₂) and organic hydroperoxides (ROOH). Therefore, in summer, the modeled OH concentrations at the surface are quite low in China, where the isoprene emissions are strong (check the anti-correlation between the isoprene and OH radical concentrations during summer in Fig. 7). Therefore, if excessive biogenic isoprene emissions were used in the CMAQ modeling, it is possible that the modeled (or virtual) NO_x levels could be higher than the actual NO_x levels due to the underestimated L_{NO_x} . In addition to isoprene, monoterpenes also convert OH to RO₂.

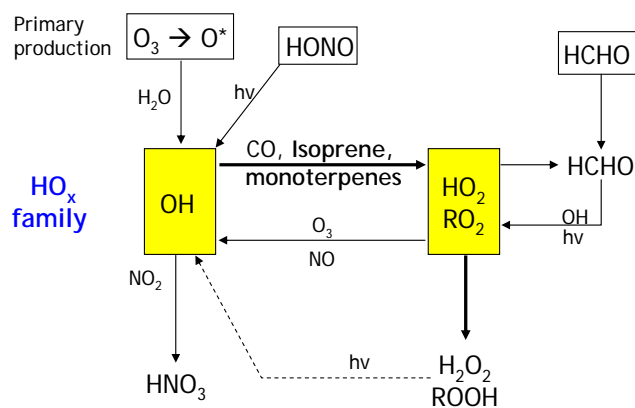


Fig. 8. An illustration of the simplified HO_x/RO₂-NO_x-biogenic VOC photochemistry.

However, the CMAQ “v4.3” model only considered the gas-phase isoprene chemistry.

As mentioned in Sect. 2.2, the GEIA emission inventory was used in this study to consider the BVOC emissions in the CMAQ modeling. In this inventory, an isoprene flux of 20.0 Tg yr⁻¹ over East Asia was estimated. However, Steiner et al. (2002) estimated an isoprene flux of only 13.6 Tg yr⁻¹ over East Asia, using the land-cover conditions derived from the AVHRR satellite. Furthermore, Fu et al. (2007) recently estimated an even lower isoprene flux of 10.8 Tg yr⁻¹ over East Asia from an inversion analysis of the GOME-retrieved HCHO columns. Overall, the isoprene flux used in this study might be approximately 1.5 to 2 times larger than those reported by Steiner et al. (2002) and Fu et al. (2007). The CMAQ-simulated HCHO (mostly, isoprene-derived in summer) columns were also compared with the GOME-retrieved HCHO columns for the summer episode (not shown). It was also found that the former is 2.23 times larger than the latter.

As indicated by previous discussions, the rates of NO_x chemical loss during summer in the CMAQ model simulations might be lower than expected, due to the low virtual OH concentrations from the use of possibly overestimated isoprene emissions in the modeling study. The rates of NO_x chemical loss were expected to be faster if the recent isoprene emissions in East Asia estimated by Fu et al. (2007) were used. Therefore, a set of sensitivity simulations of the CMAQ model were carried out with 100%, 50%, 30%, and 0% of the GEIA isoprene emissions in East Asia. The results from the sensitivity simulations are discussed at the end of this section.

In addition, the use of overestimated biogenic isoprene emissions in the CMAQ modeling can affect the NO₂/NO_x ratios. It is generally believed that there is some confidence in the ability of CTMs to simulate the actual NO₂/NO_x ratios (Martin et al., 2003). The current analysis was also based on the assumption that the actual NO₂/NO_x ratios could be successfully simulated by the CMAQ modeling (Note that the

GOME platform only measures the NO₂ columns, not the NO_x columns). Therefore, the correct NO₂ fractions are critical in this analysis (Leue et al., 2001). The NO₂/NO ratios at a pseudo-steady state can be estimated by Eq. (6):

$$\frac{[\text{NO}_2]}{[\text{NO}]} = \frac{k[\text{O}_3] + k'[\text{HO}_2] + k''[\text{CH}_3\text{O}_2] + k'''[\text{RO}_2]}{J_1} \quad (6)$$

where J_1 is the NO₂ photolysis reaction constant (s^{-1}); and k , k' , k'' , and k''' ($\text{cm}^3 \text{molecules}^{-1} \text{s}^{-1}$) are the atmospheric reaction constants for the NO-to-NO₂ conversion reactions through NO+O₃, NO+HO₂, NO+CH₃O₂, and NO+RO₂, respectively. The concentrations of HO₂ and RO₂ might also be overestimated if the biogenic isoprene levels are overpredicted using the overvalued isoprene emissions in the CMAQ modeling. This can lead to high NO₂/NO ratios in Eq. (6), which may result in incorrectly high NO₂/NO_x ratios in the CMAQ modeling.

Figure 9 shows the changes in the NO_x chemical loss rates and NO₂/NO_x ratios when 100%, 50%, 30%, and 0% of GEIA isoprene emissions were used in CMAQ modeling. (In Fig. 9, Cases I, II, III, and IV represent the CMAQ model runs that use 100%, 50%, 30%, and 0% of the GEIA isoprene emissions, respectively). The first row shows the CMAQ-calculated NO₂ levels at the surface. However, unexpectedly, the NO₂ levels at the surface increased with decreasing isoprene emissions (from Case I to IV). The second, third and fourth rows of Fig. 9 show the isoprene levels, OH radical mixing ratios, and NO₂/NO_x ratios at the surface, respectively. As shown in Fig. 9, the isoprene levels decrease continuously from Case I to IV. The OH radical concentrations increase drastically and the NO₂/NO_x ratios decrease, as expected. However, the NO₂ levels increase, as shown in Fig. 9. This is due to the formation of organic nitrates. The fifth and sixth rows show the CMAQ-estimated L_{NO_x} from Eq. (5), and the sum of the PAN and organic nitrate concentrations. As shown, the sum of PAN and organic nitrate concentrations (mostly, organic nitrates) decrease drastically with decreasing isoprene emissions, which contribute greatly to the decreases in L_{NO_x} in the fifth row of Fig. 9. In other words, the increases in L_{NO_x} due to the large increase in OH radical concentrations are offset and even partly surpassed by the decreases in L_{NO_x} due to the drastically reduced formation of organic nitrates from Case I to IV. This results in the decreasing L_{NO_x} (the fifth row) and thus the increasing NO₂ levels (the first row) from Case I to IV.

Here, it should be noted that the rates of organic nitrate formation in summer (particularly, “isoprene nitrate” formation) are highly uncertain. Many field, laboratory, and modeling studies were carried out about the formation rates, yields, and recycling rates of isoprene nitrates in summer (cf. von Kuhlmann et al., 2004; Horowitz et al., 2007; more references therein). Although the CBM4 mechanism in this study has limitation to deal with the organic nitrate formation and recycling (e.g., CBM4 does not consider the recy-

cling reactions of organic nitrates to NO₂), the above discussion has possibly important implications in comparison studies between the CTM-calculated and satellite-derived NO₂ columns (e.g., Kunhikrishnan et al., 2004; Ma et al., 2006; van Noije et al., 2006; Uno et al., 2007). For example, van Noije et al. (2006) carried out 17 global CTM ensemble simulations of tropospheric NO₂ columns, and compared the results with the GOME-retrieved NO₂ columns for the year 2000. They found similar levels and trends of the ensemble NO₂ columns over East Asia to those of this study but without considering the BVOC emissions over East Asia (at least, the coupled BVOC-NO_x chemistry was not fully discussed). Although the NO₂ levels do not vary considerably with decreasing BVOC emissions, as shown in the first row in Fig. 9, these results might be “completely coincidental” due to the effect of a factor (e.g., organic nitrate formation) offsetting that of another (e.g., OH radical concentrations). In the present sensitivity runs, van Noije et al.’s work (2006) corresponds to the fourth column in Fig. 9 (Case IV), whereas in reality, the most likely case would be the second column in Fig. 9 (Case II) according to Fu et al.’s suggestions (2007). Therefore, it should be noted that although the CTM-calculated NO₂ columns without BVOC emissions (e.g., Kunhikrishnan et al., 2004; Ma et al., 2006; van Noije et al., 2006; Uno et al., 2007) are similar to those with BVOC emissions (e.g., this study), the detailed chemistry behind the similar CTM-derived NO₂ levels would be completely different.

3.2.4 Monthly variations of NO_x emissions in East Asia

The variations in the NO_x chemical loss rates were examined. Despite considering the coupled BVOC-NO_x chemistry, the largest and smallest differences between the CMAQ-simulated and GOME-retrieved NO₂ columns were found in winter and summer, respectively. This suggests seasonal variations in NO_x emissions in East Asia.

Several studies reported that NO_x emissions from fossil fuel combustion in the United States and in East Asia are almost aseasonal (e.g., Streets et al., 2003; Jaeglé et al., 2005). Therefore, several 3-D global and regional CTM studies were carried out with constant (aseasonal) NO_x emission fluxes, and were then compared with the GOME- and/or SCIAMACHY-derived NO₂ columns (e.g., van Noije et al., 2005; Uno et al., 2007). On the other hand, several researchers recently reported that there should be monthly variations in NO_x emissions in East Asia (e.g., Kannari et al., 2007; Shin et al., 2008). In this study, the emission analysis data in East Asia was collected, and the monthly (or seasonal) variations in NO_x emissions from four major emission sectors (industry, power generation, transport, and residential sectors) in China, South Korea, and Japan were investigated. Table 2 summarizes the methodologies used for estimating the monthly-varying NO_x emissions in East Asia. In particular, in this study, the monthly variation factors from

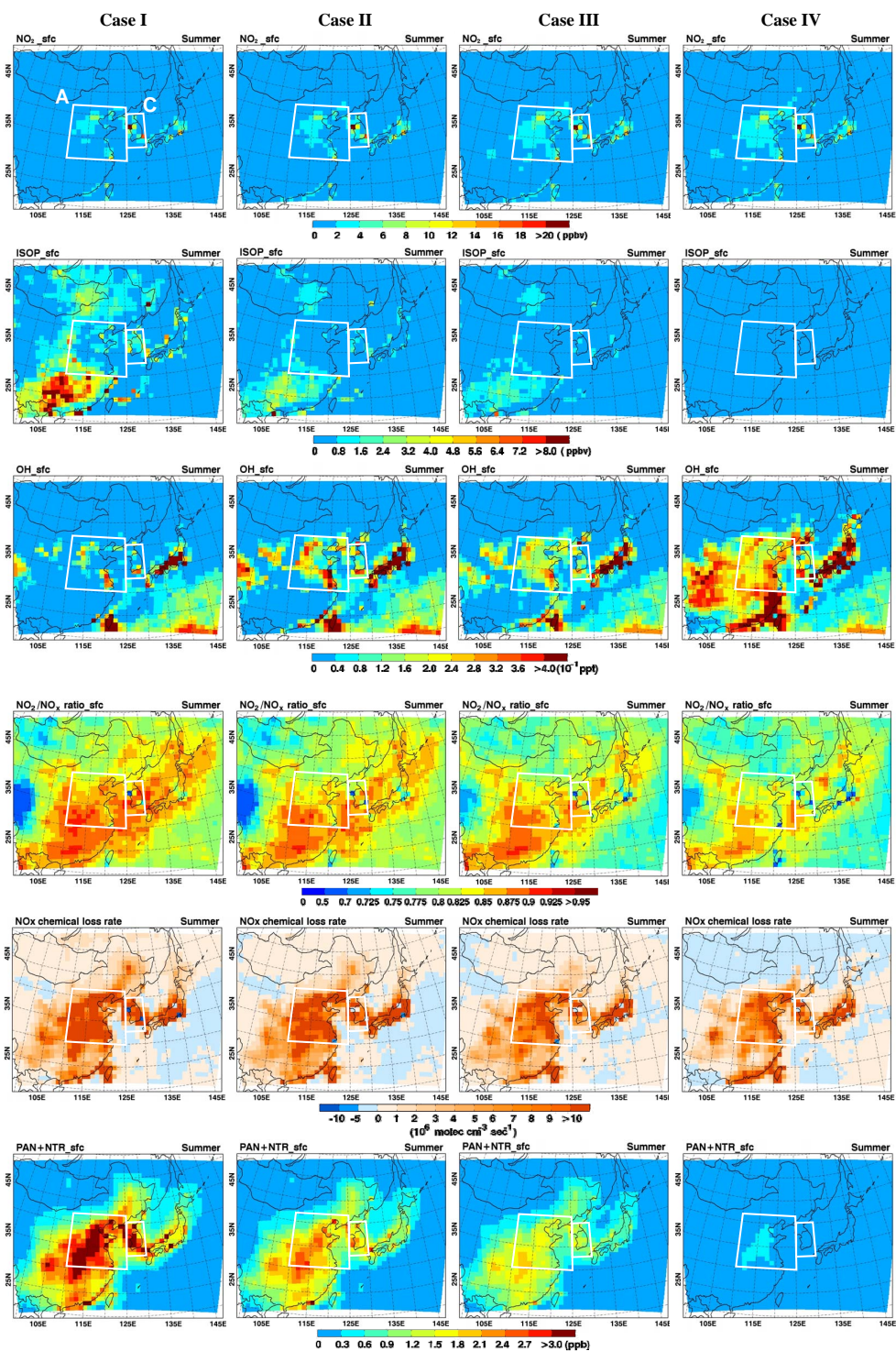


Fig. 9. Results from the sensitivity runs of the CMAQ model with 100%, 50%, 30%, and 0% of GEIA isoprene emissions (Case I, II, III, and IV, respectively): NO₂ concentrations at the surface (the first row); isoprene concentrations at the surface (the second row); OH radical concentrations (the third row); NO₂-to-NO_x ratios (the fourth row); NO_x chemical loss rates (L_{NO_x}) (the fifth row); and the sum of PAN and organic nitrate concentration (the sixth row). All concentrations were averaged between 10:00 LST and 12:00 LST. The two white boxes on the panels represent North China (A) and South Korea (C).

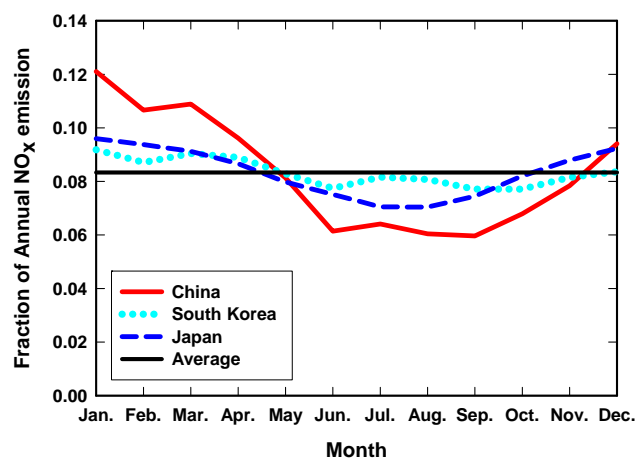
Table 2. Seasonal allocation method for anthropogenic NO_x emission fluxes in East Asia.

Region	Emission source category	Reference	Percentage of contribution of the sectors to anthropogenic NO _x emission (%)	Remark
China	Industry	EDGAR inventory	25.8	Averaging industrial combustion and industrial process
	Power	Shin (2008)	44.1	Monthly NO _x variations
	Residential	Streets et al. (2003)	5.6	–
	Transport	Streets et al. (2003); Wang et al. (2005)	24.5	–
South Korea	Industry	EDGAR inventory	15.9	Averaging industrial combustion and industrial process
	Power	Shin (2008)	18.7	Monthly NO _x variations
	Residential	Kim (1998)	4.2	–
	Transport	SMOKE factor	61.1	Road traffic survey from Korean MLTM ¹
Japan	Industry	EDGAR inventory	28.2	Averaging industrial combustion and industrial process
	Power	EDGAR inventory	4.3	EDGAR temporal factor ²
	Residential	Kim (1998)	3.7	–
	Transport	Kannari et al. (2007)	63.9	–

¹ MLTM: Ministry of Land, Transport, and Maritime; ² EDGAR temporal factors

the power generation sector were estimated from the multi-year NO_x mixing ratios measured through the Tele-Metering System (TMS: an automatic pollutant emission monitoring system) installed in the power plant (and large-scale point source) stacks (Shin, 2008). Figure 10 shows the estimated monthly variations in NO_x emissions from China, South Korea, and Japan. As shown in Fig. 10, NO_x emissions from China exhibit strong monthly variations unlike the previous estimations shown in Fig. 6. Based on this, the monthly variation factors of the NO_x emissions were applied to the Models-3/CMAQ model runs for the four seasonal episodes.

The first column of Fig. 11 shows the NO₂ columns from the CMAQ model runs with the monthly variations in NO_x emissions for the four seasonal episodes (in summer 50% of GEIA isoprene emissions were applied). The GOME-retrieved NO₂ columns and the difference between the two NO₂ columns are shown in the second and third columns in Fig. 11, respectively. As anticipated, the CMAQ-derived NO₂ columns in Fig. 11 show clearer seasonal variations than those in Fig. 3. Accordingly, the differences between the two NO₂ columns decrease. However, the general trend remains similar compared with those in Fig. 3. In Table 3, more quantitative (statistical) analysis was carried out. For example, a comparison of the values in Table 3 with those in Table 1 shows that the RMSEs are reduced by 13.9%–19.5% in

**Fig. 10.** Monthly variations in anthropogenic NO_x emissions in China, South Korea, and Japan.

North China (except for summer), biases (MBs and MNBs) still exhibiting negative.

In spite of the clearer seasonal variations in the CMAQ-simulated NO₂ columns, a summer anomaly can be still found. Unlike the cold seasons, the absolute levels of the GOME-derived NO₂ columns were reported to be low over

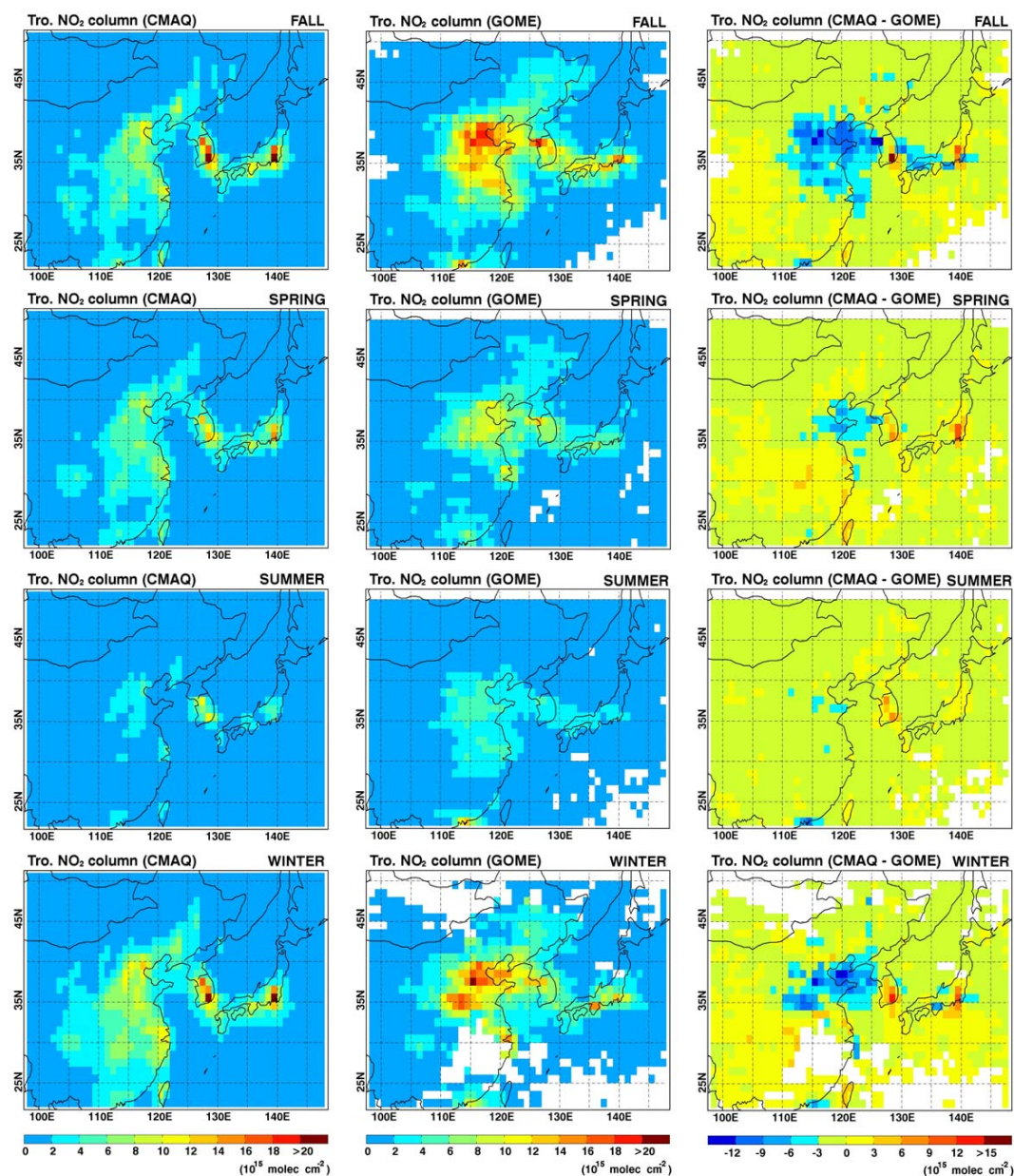


Fig. 11. As in Fig. 3, except for the CMAQ-model runs with 50% of GEIA isoprene emissions and monthly variations in anthropogenic NO_x emissions in East Asia.

North China (A) in summer ($2\text{--}6 \times 10^{15}$ molecules cm^{-2}), which is the actual and basic limitation in efforts to determine the same magnitudes of the differences between the two NO₂ columns in both the cold and warm season episodes. Since the OMI- or SCIAMACHY-derived “summer” NO₂ columns in more recent years (2007 and 2008) showed much higher NO₂ columns than those in the year 2001 ($< 2 \times 10^{16}$ molecules cm^{-2} ; not shown in this study) due to the rapid increases in NO_x emissions over East Asia, the impacts of seasonal variations in NO_x emissions on the NO₂ columns would be larger and the effects of the reduced

isoprene emissions on the NO₂ columns could be different. Hence, they should be re-evaluated for recent years in future studies.

3.2.5 Other factors affecting NO₂ columns

Two factors (NO_x chemical loss and monthly variations of NO_x emissions) that affect the CMAQ-modeled NO₂ columns were investigated. However, the GOME-derived NO₂ columns also have potential problems in the retrieval procedures, particularly in winter due to the low sun, stable boundary layer, and large aerosol concentrations (van Noije

Table 3. Statistical analysis comparing the CMAQ-simulated and GOME-derived NO₂ columns over East Asia. The CMAQ-simulated NO₂ columns were obtained from the model runs with 50% of GEIA isoprene emissions and the monthly-variations in NO_x emissions over East Asia.

			RMSE ¹	MNGE ²	MB ¹	MNB ²
CMAQ vs. GOME	A	SPRING	2.64	53.08	-1.12	-5.73
		SUMMER	1.70	50.47	-1.41	-46.58
		FALL	5.74	57.26	-4.89	-56.33
		WINTER	4.87	55.50	-3.08	-19.64
	B	SPRING	1.56	94.48	0.55	75.47
		SUMMER	1.63	42.01	-0.87	-34.08
		FALL	1.54	28.97	-0.32	0.30
		WINTER ³	–	–	–	–
	C	SPRING	2.37	30.97	0.34	4.96
		SUMMER	2.18	46.13	0.79	24.79
		FALL	4.48	38.35	-0.30	-3.86
		WINTER	3.60	44.79	1.17	23.27
	D	SPRING	1.87	99.34	0.25	66.30
		SUMMER	0.82	46.67	-0.28	-22.70
		FALL	3.10	51.91	-1.16	-21.34
		WINTER	2.53	77.22	-0.05	27.11

A: North China; B: South China; C: South Korea; D: Japan

¹ Unit, $\times 10^{15}$ molecules cm^{-2}

² Unit, %

³ Due to missing values

et al., 2006). Also, in the ACE-ASIA NO_x emission inventory, the NO_x emissions from microbiological activity in soil were not considered. On the other hand, according to a recent satellite observation-constrained top-down NO_x inventory study reported by Wang et al. (2007), the soil NO_x emissions can sometimes account for up to 43% of combustion sources during summer in China, depending on the application of fertilizers as well as seasonally variable temperatures and precipitation. A consideration of the soil NO_x emissions over North China during summer could increase the CMAQ (or CTM)-derived NO₂ levels.

Another important factor that can influence CMAQ (or CTM)-modeled NO₂ levels is the magnitude of the reaction probability of atmospheric N₂O₅ radicals ($\gamma_{\text{N}_2\text{O}_5}$). In CMAQ modeling, $\gamma_{\text{N}_2\text{O}_5}$ was determined between 0.02 and 0.002 according to Riemer et al.'s parameterizations (2003). However, the magnitude of $\gamma_{\text{N}_2\text{O}_5}$ is currently a “hotly-debated issue”, ranging from 0.1 to 0.001 (Jacob, 2000; Riemer et al., 2003; Thornton et al., 2003; Evans and Jacob, 2005; Brown et al., 2006; Davis et al., 2008; more references therein). The magnitude of $\gamma_{\text{N}_2\text{O}_5}$ is particularly important for winter-episode simulations. This is because in winter, the partitioning between NO₃ and N₂O₅ radicals shifts toward the N₂O₅ formation during the nighttime. Depending on the magnitudes of $\gamma_{\text{N}_2\text{O}_5}$ and nighttime partitioning between NO₃ and N₂O₅ radicals, the CTM-derived NO₂ levels can vary by

7%~50% (e.g. Dentener and Crutzen, 1993; Evans and Jacob, 2005; van Noije et al., 2006). Therefore, in order to predict the NO_x levels more precisely, the issue of the magnitude of $\gamma_{\text{N}_2\text{O}_5}$ requires further investigation.

3.3 Emission inventories in East Asia

3.3.1 NO_x emission inventories for South Korea

As discussed previously, it was found that the CMAQ-predicted NO₂ columns over South Korea (C) may be over-estimated by ~46.1% (based on MNGEs in Table 3) compared with the GOME-derived NO₂ columns. This finding can be partly confirmed with the emission fluxes recently released from the NIER for South Korea: CAPSS inventory. The CAPSS emission inventory for South Korea has been built up since 1999 as a part of the “Total Air Pollution Load Management System”. The CAPSS was established following the SNAP 97 (Selected Nomenclature for Air Pollution), which was used as the CORINAIR (CORE INventory of AIR emission) emission inventory system of the EEA (European Environment Agency). The CAPSS is an 1 km \times 1 km-resolved, very detailed emission inventory that employs a hybrid approach (a combination of bottom-up and top-down approaches), including intensive surveys on large-scale point sources (such as power plants, smelting facilities, and chemical & petrochemical plants), mobile sources with different automobile categories and classes, area sources with regional fuel-type consumption statistics, and non-road mobile sources such as vessels, aviation, and construction equipment. In detail, the CAPSS has the following major 11 classification codes: i) electric generating utility (EGU) combustion, ii) non-electric generating utility (NEGU) combustion, iii) industrial combustion, iv) industrial processes, v) storage and transport, vi) solvent utilization, vii) on-road mobile, viii) non-road mobile, ix) waste treatment, x) biogenic, and xi) agriculture (Heo et al., 2002; also, refer to <http://airemiss.nier.go.kr/nape/introduction/methodology/classification.jsp#>).

The annual NO_x emission fluxes of the CAPSS inventory was compared with those of two other inventories available for South Korea for 2001: ACE-ASIA and REAS. The annual NO_x emission fluxes of the REAS inventory were obtained from the official REAS emission web site (<http://www.jamstec.go.jp/frcgc/research/p3/emission.htm>). Figure 12 shows the distribution of the annual NO_x emissions of the ACE-ASIA, REAS, and CAPSS inventory for the year 2001, showing high emission fluxes in metro-city areas such as Seoul, Incheon and Busan (refer to Fig. 1, regarding the locations of these cities). Table 4 shows the NO_x emission fluxes of the CAPSS, ACE-ASIA and REAS emission inventories. The comparison shows that the annual NO_x emission fluxes of the ACE-ASIA and REAS inventories were approximately double that of the CAPSS inventory over Seoul and Incheon, and were approximately 3 times larger over

Table 4. Comparison of NO_x emissions among the CAPSS, REAS, and ACE-ASIA inventories over South Korea for 2001.

Region	ACE-ASIA (Ton yr ⁻¹)	REAS (Ton yr ⁻¹)	CAPSS (Ton yr ⁻¹)	ACE-ASIA/ CAPSS	REAS/ CAPSS
Seoul	232 059	328 256	135 771	1.71	2.42
Incheon	399 787	378 100	176 379	2.27	2.14
Busan and Ulsan	361 520	496 088	129 188	2.80	3.84
Daegu	115 438	106 483	103 422	1.12	1.03
Other region	249 236	332 832	375 032	0.66	0.89
Total	1 358 040	1 641 758	919 792	1.48	1.78

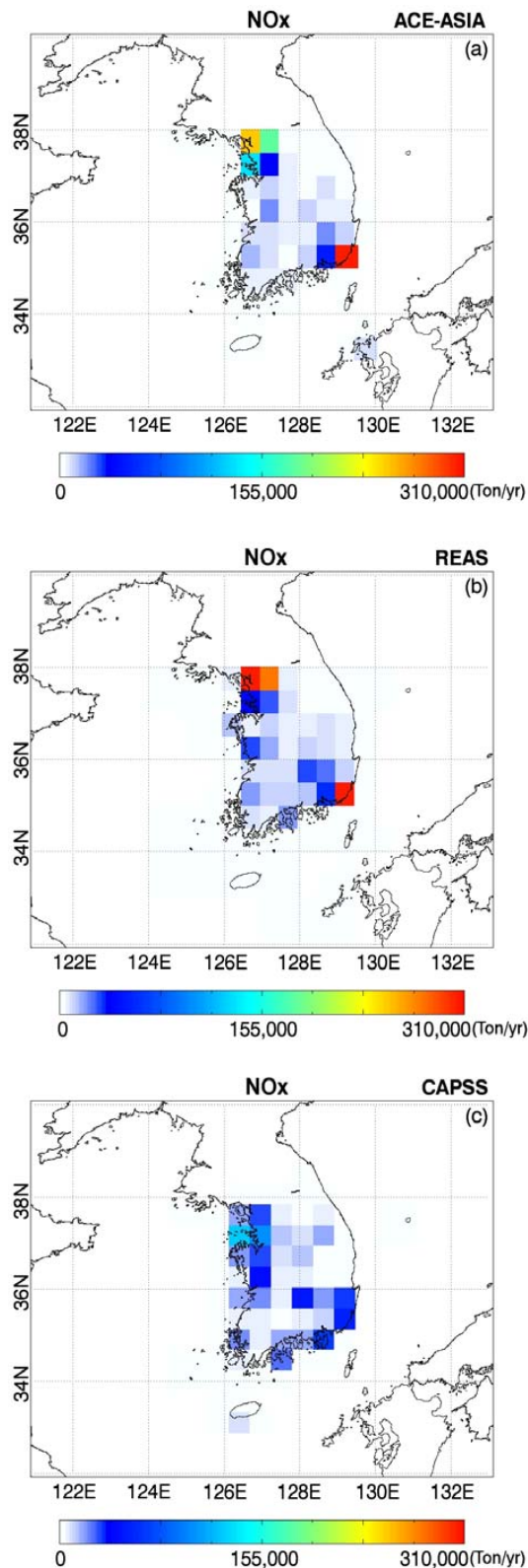
the Busan and Ulsan areas. This is in line with the conclusions drawn from a previous comparison study between the CMAQ-predicted and the GOME-derived NO₂ columns, i.e. the NO_x emission fluxes of the ACE-ASIA inventory over South Korea were overestimated. Therefore, in order to correctly consider the emissions from South Korea (C), the NO_x emissions from the ACE-ASIA and REAS inventory should be replaced by the NO_x emissions of the CAPSS inventory, and the monthly (or seasonal) variations in NO_x emissions discussed in Sect. 3.2.4 should be considered.

Figure 13 shows the CMAQ-predicted and GOME-derived NO₂ columns (the first and the second columns of Fig. 13) along with the differences between the two NO₂ columns (the third column of Fig. 13) over South Korea (C). Here, 50% of the GEIA isoprene emissions and the seasonal variations in NO_x emissions with the “CAPSS inventory” were applied to the CMAQ modeling. Based upon the comparisons between the results in Fig. 13 and Fig. 4, the degree of inconsistency become much smaller, particularly over Seoul. However, the CMAQ-simulated NO₂ columns are still larger than the GOME-derived NO₂ columns over South Korea (C) during the entire year, which suggests that the CAPSS NO_x emission fluxes can still be overestimated, particularly over the Busan areas (the second largest city in South Korea, refer to Fig. 1, regarding the location of Busan).

3.3.2 NO_x emission inventories for China

There are several NO_x emission inventories in China available for 2001 including i) ACE-ASIA/TRACE-P inventory (Streets et al., 2003), ii) REAS (Ohara et al., 2007), iii) EDGAR (Emission Database for Global Atmospheric Research) (Olivier et al., 1999, 2002), and iv) GEIA. Here, the ACE-ASIA and REAS inventories were used for a comparison study of the NO_x emission fluxes from China.

As discussed previously, when the ACE-ASIA inventory was used, the CMAQ-predicted NO₂ columns over North China (A) were underestimated by ~57.3% (based on MNGEs in Table 3), compared with the GOME-derived NO₂ columns. In order to confirm this, the three emission inventories for China were inter-compared: ACE-ASIA, REAS, and “date-back” ANL inventory. Here, the “date-back” ANL inventory was estimated based on an emission inventory de-

**Fig. 12.** Annual NO_x emission fluxes over South Korea: (a) ACE-ASIA, (b) REAS, and (c) CAPSS.

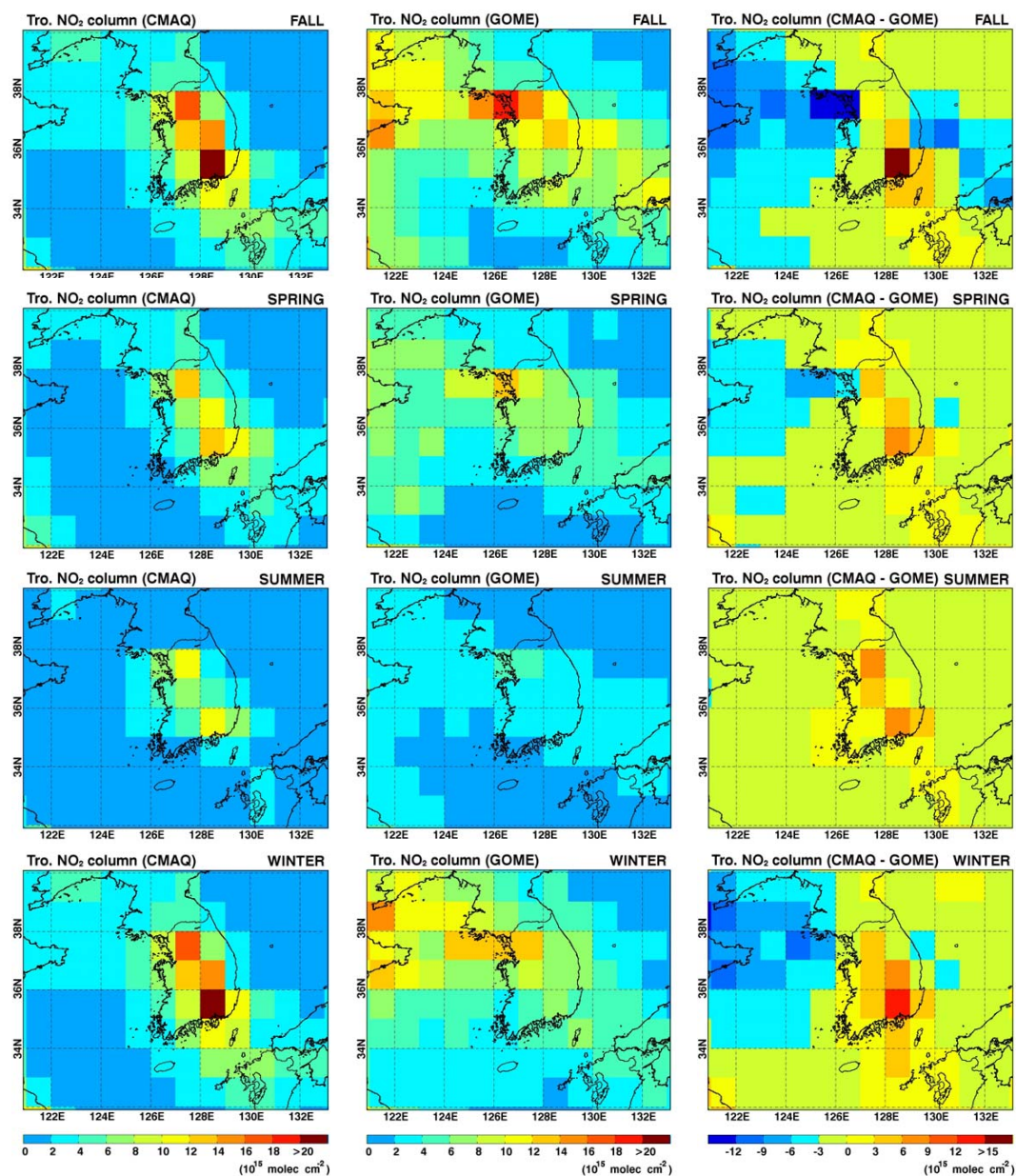


Fig. 13. As in Fig. 4, except for the CMAQ-model runs with 50% of GEIA isoprene emissions and monthly variations in anthropogenic NO_x emissions with the CAPSS inventory in South Korea.

veloped recently by Zhang et al. (2007) for 2006. The ANL inventory for 2006 is an “upgraded” and “updated” version of the ACE-ASIA emission inventory. The former (“upgraded”) indicates that the ANL inventory was improved and methodologically evolved (particularly by the considerations of small-scale combustion sources in China). The latter (“updated”) means that the ANL inventory reflects the rapidly-growing NO_x emissions from China (Zhang et al., 2007). The ANL inventory for 2006 also accounted for new emission factors, technology renewal, and bottom-up approaches for various emission sources. Since the ANL inventory is

only available for “2006”, an attempt was made to “date-back” the ANL inventory to “2001” by retaining the “upgraded” components of the ANL inventory but dating-back the “updated” parts of the ANL inventory to 2001. For this work, the NO_x emission shapes of the ANL inventory were retained but the NO_x emissions over China were reduced using China’s statistical data as well as the increase in energy and fossil fuel consumption (Zhang et al., 2007).

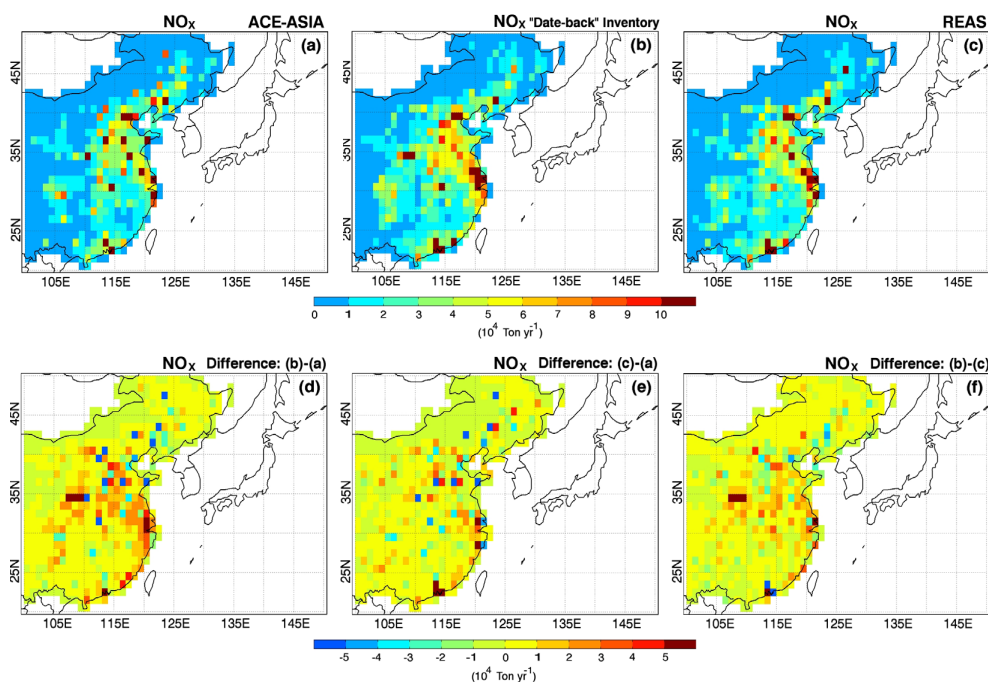


Fig. 14. Annual NO_x emissions inventory over China: (a) ACE-ASIA, (b) “date-back” ANL, and (c) REAS. The differences between the annual NO_x emission inventories are also shown in: (d) “date-back” ANL – ACE-ASIA, (e) REAS – ACE-ASIA, and (f) “date-back” ANL – REAS.

Table 5. Comparisons of NO_x emission among ACE-ASIA, “date-back” ANL, and REAS inventories over China for 2001.

Region	ACE-ASIA (Ton yr ⁻¹)	“date-back” ANL (Ton yr ⁻¹)	REAS (Ton yr ⁻¹)	“Date-back” ANL/ACE-ASIA	REAS/ACE-ASIA
North China (A)	6 063 087	6 586 730	5 995 179	1.09	0.99
South China (B)	2 145 335	2 726 533	2 609 364	1.27	1.22
Other region	2 790 983	3 521 353	2 889 506	1.26	1.04
Total	10 999 405	12 834 616	11 494 050	1.17	1.04

Figure 14 shows the annual distribution of the NO_x emission fluxes of ACE-ASIA, “date-back” ANL, and REAS inventories in the upper panels. The differences in the NO_x emission fluxes are shown in the bottom panels of Fig. 14. While the differences between the REAS and ACE-ASIA inventories (Fig. 14e) were relatively small, the differences between “date-back” ANL and ACE-ASIA inventories (Fig. 14d) and between the “date-back” ANL and REAS inventories (Fig. 14f) were relatively large. The annual NO_x emission fluxes of the ACE-ASIA inventory are smaller than those of the “date-back” ANL inventory over North China (A). This was confirmed by analyzing the NO_x emission fluxes of the ACE-ASIA, “date-back” ANL and REAS emission inventory in Table 5. The comparison shows that the NO_x emission fluxes of the “date-back” ANL inventory were ~10% larger than those of the ACE-ASIA and REAS in-

ventory over North China (A), and were approximately 30% larger than that of the ACE-AISA inventory over South China (B). The total amount of NO_x emission fluxes over North China (A) were largest in the “date-back” ANL inventory and smallest in the REAS inventory. Overall, the NO_x emission fluxes of the ACE-ASIA and REAS inventories were probably underestimated over North China (A), as was reported by Ma et al. (2006) and Uno et al. (2007). It is believed that although the annual NO_x emissions of the “date-back” ANL inventory may be the closest to the real situations for 2001, the NO_x emission fluxes of the “date-back” ANL inventory were still low based upon comparisons of the CMAQ-predicted and GOME-derived NO₂ columns, in which there was ~57.3% underestimation in NO_x emissions over North China. Again, the correct emission inventory is a critical input for examining the source-receptor relationships.

The importance of using the correct annual NO_x emission fluxes from North China for 2001 (“reference year” of the new Korean environmental policy of the “Total Air Pollution Load Management System”) to examine the impact of Chinese emissions (source) on South Korean (receptor) air quality cannot be overemphasized.

4 Summary and conclusions

This study reports on comprehensive comparisons between the CMAQ-predicted and GOME-derived NO₂ columns in order to determine the accuracy of the NO_x emission inventory over North China (A) and South Korea (C). Since both regions have a strong source-receptor relationship, an accurate knowledge of the emissions over both the regions is vital for understanding the contributions of North China emissions to South Korean air quality. When the ACE-ASIA emission inventory for 2001 was used, the CMAQ-predicted NO₂ columns were low by ~57.3% over North China (A) and high by ~46.1% over South Korea (C) compared with the GOME-derived NO₂ columns. This was further confirmed partly by comparing several emission inventories. The ACE-ASIA and REAS emission inventories showed large uncertainties over North China (A) and South Korea (C). The NO_x emission fluxes of the ACE-ASIA inventory over South Korea and North China were overestimated by ~50% and underestimated by ~10%, respectively, compared with the CAPSS and “date-back” ANL inventories. Based on these analyses, the “date-back” ANL and CAPSS inventories appear to provide a better estimation of the real situation over North China (A) and South Korea (C), respectively, even though the NO_x emissions of the “date-back” ANL inventory is still low.

This study investigated two main issues: (i) HO_x-NO_x-isoprene photo-chemistry in East Asia and (ii) seasonal variations of NO_x emissions in East Asia. The former was examined because isoprene chemistry is strongly coupled with the NO_x chemical loss rates in North China (A) and South Korea (C). In particular, the biogenic emissions of isoprene and monoterpenes are the key parameter to control OH radicals, whose concentrations can sequentially control the NO_x concentrations through nitric acid and particulate nitrate formation. Since recent studies reported lower BVOC emissions in East Asia, this study examined the impact of the BVOC emissions on the NO_x chemical loss rates (L_{NO_x}) in East Asia by relaxing the isoprene emission strengths. As expected, the OH levels increased drastically with decreasing isoprene emissions. Nevertheless, L_{NO_x} decreased slightly and the NO₂ levels increased accordingly, even with the reduced isoprene emissions. L_{NO_x} was retarded due to the less active organic nitrate formation with decreasing isoprene emissions. In addition, monthly variations in the NO_x emission fluxes over East Asia were also examined based on two facts: (i) the recent reports of monthly variations in NO_x emissions in East Asia; and (ii) the differences between CAMQ-modeled

and GOME-retrieved NO₂ columns over North China (A) are the largest in winter and smallest in summer. Although consideration of the monthly variations in NO_x emission yielded more consistent results, many issues in NO_x-related chemistry and NO_x emissions remain unclear, requiring further studies.

The correct NO_x (and BVOC) emission inventory and NO_x-related chemistry are critical for examining source-receptor relationships. Using the corrected emission inventories including the monthly variations of the NO_x emissions for North China (A) and South Korea (C), a one year-long Models-3/CMAQ modeling over East Asia is currently underway to examine and quantify more accurately the influences of Chinese (source) emissions on the South Korean (receptor) air quality.

Acknowledgements. This study was funded mainly by the Korea Ministry of Environment as an Eco-technopia 21 project under grant 121-081-055, and was also supported by the Korea Science and Engineering Foundation (KOSEF) grant (MEST) (No. R17-2008-042-01001-0).

Edited by: R. Cohen

References

- Arndt, R., Carmichael, G. R., and Roorda, J. M.: Seasonal source-receptor relationships in Asia, *Atmos. Environ.*, 32, 1397–1406, 1998.
- Binkowski, F. S. and Roselle, S. J.: Models-3 Community Multi-scale Air Quality (CMAQ) model aerosol components: 1. model description, *J. Geophys. Res.*, 108(D6), 4183, doi:10.1029/2001JD001409, 2003.
- Boersma, K. F., Eskes, H. J., and Brinksma, E. J.: Error Analysis for Tropospheric NO₂ retrieval from space, *J. Geophys. Res.*, 109, D04311, doi:10.1029/2003JD003962, 2004.
- Brown, S. S., Ryerson, T. B., Wollny, A. G., Brock, C. A., Peltier, R., Sullivan, A. P., Weber, R. J., Dube, W. P., Trainer, M., Meagher, J. F., Fehsenfeld, F. C., and Ravishankara, A. R.: Variability in nocturnal nitrogen oxide processing and its role in regional air quality, *Science*, 311, 67–70, 2006.
- Burrows, J. P., Dehn, A., Himmelmann, S., Richter, A., Voigt, S., and Orphal, J.: Atmospheric remote-sensing reference data from GOME: Part 1. Temperature-dependent absorption cross-sections of NO₂ in the 231–794 nm range, *J. Quant. Spectrosc. Ra.*, 60, 1025–1031, 1998.
- Burrows, J. P., Richter, A., Dehn, A., Deters, B., Himmelmann, S., Voigt, S., and Orphal, J.: Atmospheric remote-sensing reference data from GOME: Part 2. Temperature-dependent absorption cross-sections of O₃ in the 231–794 nm range, *J. Quant. Spectrosc. Ra.*, 61, 509–517, 1999.
- Byun, D. W. and Ching, J. K. S.: Science algorithms of the EPA models-3 Community Multiscale Air Quality (CMAQ) modeling system, EPA/600/R-99/030, US EPA, Research Triangle Park, USA.
- Byun, D. W. and Schere, K. L.: Review of the governing equations, computational algorithm, and other components of the Models-3

- Community Multi-scale Air Quality (CMAQ) Modeling system, *Appl. Mech. Rev.*, 59(2), 51–77, 2006.
- CAPSS (Clean Air Policy Support System): National Institute of Environmental Research (NIER), Clean Air Policy Support System 3rd final report, South Korea, 2003.
- Chance, K.: Analysis of BrO measurements from the Global Ozone Monitoring Experiment, *Geophys. Res. Lett.*, 27, 3335–3338, 1998.
- Colella, P. and Woodward, P. L.: The Piecewise Parabolic Method (PPM) for gas dynamical simulation, *J. Comput. Phys.*, 54, 174–201, 1984.
- Davis, J. M., Bhavsar, P. V., and Foley, K. M.: Parameterization of N₂O₅ reaction probabilities on the surface of particles containing ammonium, sulfate, and nitrate, *Atmos. Chem. Phys.*, 8, 5295–5311, 2008, <http://www.atmos-chem-phys.net/8/5295/2008/>.
- Dentener, F. J. and Crutzen, P. J.: Reaction of N₂O₅ on tropospheric aerosols: Impact on the global distribution of NO_x, O₃, and OH levels, *J. Geophys. Res.*, 98, 7149–7163, 1993.
- Draxler, R. R. and Hess, G. D.: An overview of the HYSPLIT-4 modeling system for trajectories, dispersion, and deposition, *Aust. Meteorol. Mag.*, 17, 295–308, 1998.
- Evans, M. J. and Jacob, D. J.: Impact of new laboratory studies of N₂O₅ hydrolysis on global model budgets of tropospheric nitrogen oxides, ozone, and OH, *Geophys. Res. Lett.*, 32, L09813, doi:10.1029/2005GL022469, 2005.
- Fahey, K. M. and Pandis, S. N.: Size-resolved aqueous-phase atmospheric chemistry in a three-dimensional chemical transport model, *J. Geophys. Res.*, 108(D22), 4690, doi:10.1029/2003JD003564, 2003.
- Fu, T., Jacob, D. J., Palmer, P. I., Chance, K., Wang, Y. X., Barletta, B., Blake, D. R., Statton, J. C., and Pilling, M. J.: Space-based formaldehyde measurements as constraints on volatile organic compound emissions in east and south Asia and implications for ozone, *J. Geophys. Res.*, 112, D06312, doi:10.1029/2006JD007853, 2007.
- Gery, M. W., Whitten, G. Z., Killus, J. P., and Dodge, M. C.: A photochemical kinetics mechanism for urban and regional scale computer modeling, *J. Geophys. Res.*, 94, 12 925–12 956, 1989.
- Greenblatt, G. D., Orlando, J. J., Burkholder, J. B., and Ravishankara, A. R.: Absorption measurements of oxygen between 330 and 1140 nm, *J. Geophys. Res.*, 95, 18 577–18 582, 1990.
- He, Y., Uno, I., Wang, Z., Ohara, T., Sugimoto, N., Shimizu, A., Richter, A., and Burrows, J. P.: Variations of the increasing trend of tropospheric NO₂ over central east China during the past decade, *Atmos. Environ.*, 41, 4865–4876, 2007.
- Heo, J. S., Lee, D. K., Hong, J. H., Seok, K. S., Lee, D. G., and Eom, Y. S.: A proposal on the new air emission source categories, *J. KOSAE*, 18(3), 231–245, 2002.
- Horowitz, L. W., Fiore, A. M., Milly, G. P., Cohen, R. C., Perring, A., Wooldridge, P. J., Hess, P. G., Emmons, L. K., and Lamarque, J.-F.: Observational constraints on the chemistry of isoprene nitrates over the eastern United States, *J. Geophys. Res.*, 112, D12S08, doi:10.1029/2006JD007747, 2007.
- Jacob, D. J.: Heterogeneous chemistry and tropospheric ozone, *Atmos. Environ.*, 34, 2131–2159, 2000.
- Jaeglé, L., Steinberger, L., Martin, R. V., and Chance, K.: Global partitioning of NO_x sources using satellite observations: Relative roles of fossil fuel combustion, biomass burning and soil emissions, *Faraday Discuss.*, 130, 407–423, 2005.
- Kannari, A., Tonooka, Y., Baba, T., and Murano, K.: Development of multi-species 1 km×km resolution hourly basis emissions inventory for Japan, *Atmos. Environ.*, 41, 3428–3439, 2007.
- Kato, N. and Akimoto, H.: Anthropogenic emissions of SO₂ and NO_x in Asia: Emission inventories, *Atmos. Environ.*, 41, S171–S191, 2007.
- Kim, D. Y.: Development of a grided, hourly and speciated air pollutant emission modeling system, Ph.D. thesis, Seoul National University, Seoul, Korea, 1998.
- Koelemeijer, R. B. A., Stammes, P., Hovenier, J. W., and de Haan, J. F.: A fast method for retrieval of cloud parameters using oxygen A band measurements from the Global Ozone Monitoring Instrument, *J. Geophys. Res.*, 106(D4), 3475–3490, 2001.
- Korean Ministry of Environment: Execution of special measurements to improve metropolitan atmospheric Environment, Korea Environmental Policy Bulletin, IV(1), 1–15, 2006.
- Kunhikrishnan, T., Lawrence, M. G., von Kuhlmann, R., Richter, A., Ladstätter-Weissenmayer, A., and Burrows, J. P.: Analysis of tropospheric NO_x over Asia using the model of atmospheric transport and chemistry (MATCH-MPIC) and GOME-satellite observations, *Atmos. Environ.*, 38, 581–596, 2004.
- Leue, C., Wenig, M., Wagner, T., Klimm, O., Platt, U., and Jähne, B.: Quantitative analysis of NO_x emissions from global Ozone Monitoring Experiment satellite image sequences, *J. Geophys. Res.*, 106(D6), 5493–5505, 2001.
- Ma, J., Richter, A., Burrows, J. P., Nüß, H., and van Aardenne, J. A.: Comparison of simulated tropospheric NO₂ over China with GOME satellite data, *Atmos. Environ.*, 40, 593–604, 2006.
- Martin, R. V., Jacob, D. J., Chance, K., Kurosu, T. P., Palmer, P. I., and Evans, M. J.: Global inventory of nitrogen oxide emissions constrained by space-based observation of NO₂ columns, *J. Geophys. Res.*, 108(D17), 4537, doi:10.1029/2003JD003453, 2003.
- Ohara, T., Akimoto, H., Kurokawa, J., Horii, N., Yamaji, K., Yan, X., and Hayasaka, T.: An Asian emission inventory of anthropogenic emission sources for the period 1980–2020, *Atmos. Chem. Phys.*, 7, 4419–4444, 2007, <http://www.atmos-chem-phys.net/7/4419/2007/>.
- Olivier, J. G. J., Bloos, J. P. J., Berdowski, J. J. M., Visschedijk, A. J. H., and Bouwman, A. F.: A 1990 global emission inventory of anthropogenic sources of carbon monoxide on 1°×1° developed in the framework of EDGAR/GEIA, *Chemosphere, Global Change Science*, 1, 1–17, 1999.
- Olivier, J. G. J., Berdowski, J. J. M., Peters, J. A. H. W., Bakker, J., Visschedijk, A. J. H., and Bloos, J. P. J.: Applications of EDGAR: emission database for global atmospheric research, Report on: 410.200.051. RIVM, The Netherlands, 1–142, 2002.
- Pandis, S. N. and Seinfeld, J. H.: Sensitivity Analysis of a chemical mechanism for aqueous-phase atmospheric chemistry, *J. Geophys. Res.*, 94(D1), 1105–1126, 1989.
- Richter, A. and Burrows, J. P.: Retrieval of tropospheric NO₂ from GOME measurements, *Advance in Space Research*, 29, 16 673–16 683, 2002.
- Richter, A., Burrows, J. P., Nüß, H., Granier, C., and Niemeier, U.: Increase in tropospheric nitrogen dioxide over China observed from space, *Nature*, 437, 129–132, 2005.
- Riemer, N., Vogel, H., Vogel, B., Schell, B., Ackermann, I., Kessler, C., and Hass, H.: Impact of the heterogeneous hydrolysis of N₂O₅ on chemistry and nitrate aerosol formation in

- the lower troposphere under photosmog conditions, *J. Geophys. Res.*, 108(D4), 4144, doi:10.1029/2002JD002436, 2003.
- Rothman, L. S., Gamache, R. R., Tipping, R. H., Rinsland, C. P., Smith, M. A. H., Benner, D. C., Devi, V. M., Flaud, J. M., Camy-Peyret, C., Perrin, A., Goldman, A., Massie, S. T., Brown, L. R., and Toth, R. A.: The HITRAN molecular database: editions of 1991 and 1992, *J. Quant. Spectrosc. Ra.*, 48, 469–507, 1992.
- Roazanov, V., Diebel, D., Spurr, R. J. D., and Burrows, J. P.: GOME-TRAN: A radiative transfer model for the satellite project GOME – the plane parallel version, *J. Geophys. Res.*, 102, 16683–16695, 1997.
- Schwartz, S. E.: Mass transport considerations pertinent to aqueous-phase reactions of gases in liquid-water clouds, *Chemistry of Multiphase Atmospheric System*, edited by: Jaeschke, W., Springer-Verlag, Berlin, 415–471, 1986.
- Shin, W. G.: Impact analysis of emission estimation improvements and emission reduction scenarios for large point sources in support of Cap and Trade program of the Seoul Metropolitan Areas, Ph.D. thesis, Konkuk University, Seoul, Korea, 1–166, 2008.
- Song, C. H., Chen, G., Hanna, S. R., Crawford, J., and Davis, D. D.: Dispersion and chemical evolution of ship plumes in the marine boundary layer: Investigation of O₃/NO_y/HO_x chemistry, *J. Geophys. Res.*, 108(D4), 4143, doi:10.1029/2002JD002216, 2003.
- Song, C. H., Park, M. E., Lee, K. H., Ahn, H. J., Lee, Y., Kim, J. Y., Han, K. M., Kim, J., Ghim, Y. S., and Kim, Y. J.: An investigation into seasonal and regional aerosol characteristics in East Asia using model-predicted and remotely-sensed aerosol properties, *Atmos. Chem. Phys.*, 8, 6627–6654, 2008, <http://www.atmos-chem-phys.net/8/6627/2008/>.
- Stauffer, D. R. and Seaman, N. L.: Use of four-dimensional data assimilation in a limited-area mesoscale model. Part I: experiments with synoptic-scale data, *Mon. Weather Rev.*, 118(6), 1250–1277, 1990.
- Stauffer, D. L. and Seaman, N. L.: Multiscale four-dimensional data assimilation, *J. Appl. Meteorol.*, 33(3), 416–434, 1994.
- Steiner, A., Luo, C., Huang, Y., and Chameides, W. L.: Past and present-day biogenic volatile organic compound emissions in East Asia, *Atmos. Environ.*, 36, 4895–4905, 2002.
- Streets, D. G., Bond, T. C., Carmichael, G. R., Fernandes, S. D., Fu, Q., He, D., Klimont, Z., Nelson, S. M., Tsai, N. Y., Wang, M. Q., Woo, J.-H., and Yarber, K. F.: An inventory of gaseous and primary aerosol emissions in Asia in the year 2000, *J. Geophys. Res.*, 108(D21), 8809, doi:10.1029/2002JD003093, 2003.
- Thornton, J. A., Braban, C. F., and Abbatt, J. P. D.: N₂O₅ hydrolysis on submicron organic aerosol: The effect of relative humidity, particle phase, and particle size, *Phys. Chem. Chem. Phys.*, 5(20), 4593–4603, 2003.
- Uno, I., He, Y., Ohara, T., Yamaji, K., Kurokawa, J.-I., Katayama, M., Wang, Z., Noguchi, K., Hayashida, S., Richter, A., and Burrows, J. P.: Systematic analysis of interannual and seasonal variations of model-simulated tropospheric NO₂ in Asia and comparison with GOME-satellite data, *Atmos. Chem. Phys.*, 7, 1671–1681, 2007, <http://www.atmos-chem-phys.net/7/1671/2007/>.
- van Noije, T. P. C., Eskes, H. J., Dentener, F. J., Stevenson, D. S., Ellingsen, K., Schultz, M. G., Wild, O., Amann, M., Atherton, C. S., Bergmann, D. J., Bey, I., Boersma, K. F., Butler, T., Co-fala, J., Drevet, J., Fiore, A. M., Gauss, M., Hauglustaine, D. A., Horowitz, L. W., Isaksen, I. S. A., Krol, M. C., Lamarque, J.-F., Lawrence, M. G., Martin, R. V., Montanaro, V., Miller, J.-F., Pitari, G., Prather, M. J., Pyle, J. A., Richter, A., Rodriguez, J. M., Savage, N. H., Strahan, S. E., Sudo, K., Szopa, S., and van Roozendael, M.: Multi-model ensemble simulations of tropospheric NO₂ compared with GOME retrievals for the year 2000, *Atmos. Chem. Phys.*, 6, 2943–2979, 2006, <http://www.atmos-chem-phys.net/6/2943/2006/>.
- von Kuhlmann, R., Lawrence, M. G., Pöschl, U., and Crutzen, P. J.: Sensitivities in global scale modeling of isoprene, *Atmos. Chem. Phys.*, 4, 1–17, 2004, <http://www.atmos-chem-phys.net/4/1/2004/>.
- Vountas, M., Roazanov, V., and Burrows, J.: Ring effect: Impact of rotational Raman scattering on radiative transfer in earth's atmosphere, *J. Quant. Spectrosc. Ra.*, 60, 943–961, 1998.
- Wang, X., Mauzerall, D. L., Hu, Y., Russell, A. G., Larson, E. D., Woo, J. H., Streets, D. G., and Guenther, D. G.: A high resolution emission inventory for eastern China in 2000 and three scenarios for 2020, *Atmos. Environ.*, 39, 5917–5933, 2005.
- Wang, Y., McElroy, M. B., Martic, R. V., Streets, D. G., Zhang, Q., and Fu, T. M.: Seasonal variability of NO_x emissions over east China constrained by satellite observations: Implications for combustion and microbial sources, *J. Geophys. Res.*, 112, D06301, doi:10.1029/2006JD007538, 2007.
- Wesely, M. L.: Parameterization of surface resistances to gaseous dry deposition in regional-scale numerical models, *Atmos. Environ.*, 23, 1293–1304, 1989.
- Zhang, Q., Streets, D. G., He, K., Wang, Y., Richter, A., Burrows, J. P., Uno, I., Jang, C. J., Chen, D., Yao, Z., and Lei, Y.: NO_x emission trends for China, 1995–2004: The view from the ground and the view from space, *J. Geophys. Res.*, 112, D22306, doi:10.1029/2007JD008684, 2007.